Cement and Concrete Research 40 (2010) 851–866

Contents lists available at ScienceDirect

Cement and Concrete Research

journal homepage: http://ees.elsevier.com/CEMCON/default.asp

Chemical model for cement-based materials: Temperature dependence of thermodynamic functions for nanocrystalline and crystalline C–S–H phases

Ph. Blanc [a,*], X. Bourbon [b], A. Lassin [a], E.C. Gaucher [a]

[a] BRGM, 3 Avenue Claude Guillemin, 45060 Orléans Cedex 2, France
[b] ANDRA — Scientific Division, 1–7 Rue Jean Monnet, Parc de la Croix Blanche, 92298 Chatenay Malabry Cedex, France

ARTICLE INFO

Article history:
Received 23 February 2009
Accepted 8 December 2009

Keywords:
Calcium–silicate–hydrate (C–S–H) B
Thermodynamic calculations B
Temperature A

ABSTRACT

In the context of waste confinement and, more specifically, waste from the nuclear industry, concrete is used both as a confinement and as a building material. Its exposure to high temperatures makes its geochemical behavior difficult to predict over large periods of time. The present work aims to elucidate the solubility constants, as a function of temperature, for the phases of the system $CaO–SiO_2–H_2O$. For the nanocrystalline phases, the present work investigates the existence of compounds of fixed composition, possibly in a metastable state. The question of whether the nanocrystalline C–S–H phases correspond to a series of phases of discrete composition or a solid solution is discussed and compared to the possible influence of impurities in the solid phases.

For the crystalline phases, having established that the currently available values of thermodynamic properties were not consistent, we show that their refinement leads to a better agreement with the literature data. From the refined thermodynamic properties of crystalline C–S–H, a polyhedral decomposition model is developed. It enables to estimate the enthalpy of formation and the heat capacity of nanocrystalline C–S–H phases. Finally, verification shows that such phases remain unstable compared to the crystalline phases, at room or higher temperatures. A comparison, based on reaction enthalpies derived from experimental data indicates that predicted values for nanocrystalline C–S–H are in close agreement with experimental data. By estimating the properties of okenite and truscottite with the model developed in this study, we have been able to complete the $CaO–SiO_2–H_2O$ phase diagram with a reasonable agreement with the literature. The case of jaffeite remains open to discussion. Finally, for the hydrate C2SH,α, the model predicts a transition with hillebrandite at 159 °C, in contradiction with the hypothesis of C2SH,α metastability.

1. Introduction

Many works have been published to date concerning the equilibria between solids and aqueous solutions in cementitious media. The applications concern different domains like the improvement of the formulation of concretes, the durability of cementitious materials in response to different types of physical and chemical aggressions or, more recently, environmental applications related to the stabilization of waste and the use of concretes as confinement materials. Among the latter, a special case relates to underground buildings for HAVL (high activity long-lived) radioactive waste disposal. Concrete is there used as a supporting material for the access galleries [1,2]. Concrete is also used as a confinement material for MAVL (medium activity long-lived) waste [3]). The durability of these cementitious barriers and the consequences of the interaction with other confinement materials are still widely discussed [4].

The present work is based on a selection of the cementitious phases of interest for deep storage [5]. It is specially focused on the minerals belonging to the $CaO–SiO_2–H_2O$ (C–S–H) chemical system. It aims at defining the solubility constants of the minerals that compose cement pastes, based on the most recent works on this subject and in agreement with the thermodynamic databases of ANDRA (Thermochimie6, [6]) and BRGM (Thermoddem, [7]). Since some wastes are exothermic, the model must be able to take into account a range of temperatures from 10 to 100 °C. This implies to develop a thermodynamic database including not only the equilibrium constant at room temperature but also the enthalpy of formation and the heat capacity function.

Among all of the solubility models published to date for nanocrystalline C–S–H, two large families may be distinguished: those for which the C–S–H are present as discrete phases [8,9] and those for which the C–S–H are considered as phases with a continually variable composition [10–12].

The influence of temperature is usually not taken into account in this type of model. For nanocrystalline C–S–H, the double solid solution proposed by Lothenbach et al. [125] remains an exception.

* Corresponding author. Tel.: +33 2 38 64 39 92; fax: +33 2 38 64 30 62.
E-mail address: p.blanc@brgm.fr (P. Blanc).

0008-8846/$ – see front matter © 2009 Elsevier Ltd. All rights reserved.
doi:10.1016/j.cemconres.2009.12.004

Even for crystalline C–S–H, little solubility data is available beyond 25 °C. Indeed, the solubility of phases of the system $CaO–SiO_2–H_2O$ has been studied at 55 and 85 °C by Dickson et al. [13] and by Glasser et al. [14] and at 90 °C by Courault [15]. Paul and Glasser [16] have characterized the mineralogical transformations in a concrete held at 85 °C during 10 years. However, few geochemical models actually take into account the temperature influence on cementitious material models. One may cite in particular the model developed by Thomas et al. [17], based on a simplified mineralogy since only the portlandite, gypsum, ettringite and monosulfate phases are considered. Recently, an important work by Matschei et al. [123] had provided new solubility data (including temperature dependence) for a large set of minerals belonging to the cementitious chemical system. Based on those experiments, Lothenbach et al. [121,124] have proposed their own solubility model.

The present work aims in collecting the experimental data available for the solubility of C–S–H phases at 25 °C and at $T>25$ °C, making use of the experimental works already published. The latter are integrated in a polyhedral decomposition model that provides an estimate of the enthalpy of formation and of the heat capacity of minerals when such parameters are not available. The final selection of thermodynamic properties is organized the following way:

- when available, properties are taken from already published, experimental works (case of the formation enthalpy for some crystalline C–S–H)
- equilibrium constants for nanocystalline C–S–H are extracted from a set of experimental data. The case is different than before because even the composition of C–S–H phases is derived from the datasets
- for crystalline C–S–H, the properties datasets are completed with the results of the phase diagram refinement
- the lacking properties are estimated with the polyhedral model.

2. Context and theoretical tools

This section is devoted to a discussion covering the thermodynamic database and the conventions used throughout the text.

2.1. Context of selecting thermodynamic data

The thermodynamic properties of many aqueous complexes have been previously collected and selected for the ANDRA (Thermochimie6) and BRGM (Thermoddem) databases [6]. The Thermochimie6 database has been developed to meet the needs of ANDRA in terms of geochemical modeling, whereas the Thermoddem database has been designed in order to cover the field of waste (municipal or industrial) disposal.

The two databases relies on CODATA recommendations [18] for the basis species and the reference states of elements. Recent advances have been made, in particular for aluminum and silicon [19,20,31,32], which led us to modify the properties of formation of the aqueous species Al^{+++} and H_4SiO_4 [29,30]. The two databases have adopted NEA recommendations [21–23], particularly as for the influence of ionic strength and temperature.

For the remainder of this work, the basis species for writing equilibria reactions are Al^{+++}, Ca^{++}, H_4SiO_4, H_2O and H^+. The convention chosen for the standard state of compounds is that proposed by Helgeson et al. [24]. The reference conditions, following IUPAC recommendations [25], are set at 298.15 K (25 °C) and 0.1 MPa (1 bar). These reference conditions have also been adopted by CODATA [26].

The minerals/solution equilibria in this work were calculated using PHREEQC software [27], using the extended Debye–Hückel activity model.

Table 1 gives the list of the complexes used for this study. The selection criteria are explained in Blanc et al. [6].

2.2. Equations and notations used

The temperature, pressure and energy units adopted in the formula are respectively the Kelvin, Pascal and Joule, in accordance with the International System of Units. However, Celsius degrees are used in the text and the illustrations, following accepted practice.

Considering a phase AB, when the reaction $AB \rightarrow A^+ + B^-$ reaches the equilibrium at P_r and T_r (pressure and temperature of reference), the ion activity product IAP_{AB} becomes equal to the equilibrium constant:

$$K_{AB}(T_r) = IAP_{AB} = (A^+)\cdot(B^-) = \gamma_{A^+}\cdot[A^+]\cdot\gamma_{B^-}\cdot[B^-] \quad (1)$$

where (A^+), $[A^+]$ and γ_{A+} correspond respectively to the activity, the concentration and the activity coefficient of the cation A^+. $K_{AB}(T_r)$ is related to the standard free enthalpy of reaction $\Delta_r G^0_{AB,Pr,Tr}$ by the following relation:

$$\Delta_r G^0_{AB,Pr,Tr} = -R\cdot T_r\cdot \log K_{AB,Pr,Tr}\cdot \ln(10) \quad (2)$$

where $R = 8.314472\ \mathrm{J\ mol^{-1}K^{-1}}$ is the gas constant.

The standard free enthalpy of reaction is obtained by subtracting the standard free enthalpy of formation of the mineral phase considered and those of the aqueous species involved in the reaction. According to the convention of Helgeson et al. [28], it is possible to consider, for this calculation, the apparent standard free enthalpy $\Delta_f G^0_{AB,P,T}$ which corresponds to the relation:

$$\begin{aligned}\Delta_f G^0_{AB,P,T} &= \Delta_f H^0_{AB,P,T} - T\cdot\Delta_f S^0_{AB,P,T}\\ &= \Delta_f H^0_{AB,Pr,Tr} - T\cdot\Delta_f S^0_{AB,Pr,Tr} + \int_{T_r}^{T} Cp_{AB}\,dT - T\cdot\int_{T_r}^{T}\frac{Cp_{AB}}{T}\,dT\\ &\quad + \int_{P_r}^{P} V_{AB}\,dP\end{aligned} \quad (3)$$

where: $T_r = 298.15$ K; $P_r = 0.1$ Mpa or 1 bar

$\Delta_f H^0_{AB,P,T}$ enthalpy of formation of the phase AB, at temperature T and pressure P

$\Delta_f S^0_{AB,Pr,Tr} = S^0_{AB,Pr,Tr} - \sum S^0_{elts,Pr,Tr}$ entropy of formation of phase AB; S^0_{AB} the third law entropy of the phase AB, at temperature T_r and pressure P_r

Cp_{AB} heat capacity of the phase AB

V_{AB} molar volume of the phase AB, independent of temperature

Equilibrium constants are calculated along the liquid–vapor saturation curve. According to the convention of Helgeson et al. [24], the liquid–vapor saturation pressure P_{sat} is the reference pressure, i.e. 0.1 MPa, from 273.15 to 373.15 K (0 to 100 °C). Beyond 373.15 K, P_{sat} follows the liquid–water vapor saturation curve. The heat capacity function corresponds to the Maier–Kelley relation:

$$Cp(T)_{AB} = a_{AB} + b_{AB}\cdot T - c_{AB}/T^2 \quad (4)$$

where a_{AB}, b_{AB} and c_{AB} are the Maier–Kelley coefficients of the phase AB. Relations (3) and (4) may be combined as follows:

$$\begin{aligned}\Delta_f G^0_{AB,P,T} &= \Delta_f G^0_{AB,Pr,Tr} - S^0_{AB,Pr,Tr}\cdot(T-T_r)\\ &\quad + a_{AB}\cdot[T - T_r - T\cdot\ln(T/T_r)] - b_{AB}\cdot(T-T_r)^2/2 - c_{AB}\cdot(T-T_r)^2/(2\cdot T^2\cdot T_r)\\ &\quad + \int_{P_r}^{P} V_{AB}\,dP\end{aligned} \quad (5)$$

Table 1
Thermodynamic properties of aqueous complexes and elements in their reference state.

Phase	$LogK_{Pr,Tr}$	$\Delta_f G^0_{Pr,Tr}$ (kJ mol^{-1})	$\Delta_f H^0_{Pr,Tr}$ (kJ mol^{-1})	$S^0_{Pr,Tr}$ (J mol^{-1} K^{-1})	Reference	Cp(298) (J mol^{-1} K^{-1})	Reference and method used for calculating the Cp
System H_2O							
H_2O	(*)	−237.14	**−285.83**	**69.95**	[18,40]	**75.35**	State equation published by IAPW [40]
O_2,aq	−85.99	16.53	**−12.13**	**109.00**	[33]	**234.30**	From the HKF coefficients of [33]
H_2,aq	−3.08	17.56	**−4.20**	**57.70**	[38]	**166.94**	From the HKF coefficients of [33]
H^+	(*)	0.00	**0.00**	**0.00**	By convention, [18]	**0.00**	By convention, [18]
OH^-	−14.00	−157.22	**−230.02**	**−10.90**	[18]	**−137.19**	From the HKF coefficients of [34]
e−	(*)	0.00	**0.00**	**65.34**	By convention, [18]	**14.42**	By convention, [18]
Silica complexes							
$H_4SiO_{4,aq}$	(*)	−1309.23	**−1461.19**	**180.77**	See text	**198.86**	See text
$H_2SiO_4^{-2}$	**−23.14**	−1177.14	**−1386.72**	−12.58	[39]	**−80.00**	[36]
$Ca(H_3SiO_4)^+$	**−8.83**	−1811.63	−1972.56	**61.62**	[37]	**212.88**	From the HKF coefficients of [37]
$H_3(SiO_4)^-$	**−9.84**	−1253.06	−1431.83	**90.87**	[37]	**−12.51**	From the HKF coefficients of [37]
Calcium complex							
$CaOH^+$	**−12.78**	−717.00	−751.62	**28.00**	[18]	**5.86**	From the HKF coefficients of [35]
Elements in their reference state, at 25 °C and 1 bar							
O_2,g	−83.09	0.00	**0.00**	**205.15**	[18]	**29.38**	Value at 25 °C [18]
H_2,g	0.00	0.00	**0.00**	**130.68**	[18]	**28.84**	Value at 25 °C [18]
Si,cr	−63.19	0.00	**0.00**	**18.81**	[18]	**19.79**	Value at 25 °C [18]
Ca,cr	−96.85	0.00	**0.00**	**41.59**	[18]	**25.93**	Value at 25 °C [18]

Bold type: reference property; (*) primary master species.

For a constant heat capacity Cp_{AB}, the relation (5) comes to:

$$\Delta_f G^0_{AB,P,T} = \Delta_f G^0_{AB,Pr,Tr} - S^0_{AB,Pr,Tr}\cdot(T-T_r) + a_{AB}\cdot[T-T_r-T\cdot\ln(T/T_r)] + \int_{P_r}^{P} V_{AB}\,dP \quad (6)$$

For the mineral phases, we will consider the molar volume independent of the pressure and the volume. The integral term related to the molar volume in relation (6) then becomes $\int_{Pr}^{P} V_{AB}dP = V_{AB}\cdot(P-P_r)$.

Finally, following accepted practice, we have used cementitious notations to designate some phases, i.e. C=CaO, S=SiO_2 and H=H_2O. Mineral stoichiometries and equilibrium reactions considered in this work are reported in Table 2.

3. C–S–H solubility

Crystalline C–S–H is stable at high temperature, which favors crystallization [41]. At room temperature, the polymerization of tetrahedral SiO_2 is slowed down and leads to nanocrystalline phases. It first produces dimers then pentamers [42,43]. Polymerization accelerates with increasing temperature [44], all the more easily as the C/S ratio is small [45].

3.1. Nanocrystalline C–S–H

3.1.1. Introduction

Two different types of solubility models have been developed for C–S–H. Indeed, C–S–H are considered either as discrete composition phases [8,9], or with a continuous variable composition [10–12,124,125]. In fact, Jennings [10] and Berner's model [11] lies between both categories as Jennings [10] has actually defined a relationship between Ca and Si concentration in solution whereas Berner [11] has

Table 2
Stoichiometry and reactions considered in the present study.

Mineral	Formula	Reaction
Crystalline C–S–H		
Okenite	$CaSi_2O_4(OH)_2.H_2O$	$CaSi_2O_4(OH)_2\cdot H_2O + 2H^+ + 1H_2O = Ca^{++} + 2H_4SiO_4$
Gyrolite	$Ca_2Si_3O_7(OH)_2.2H_2O$	$Ca_2Si_3O_7(OH)\cdot 2H_2O + 4H^+ + 1.5H_2O = 2Ca^{++} + 3H_4SiO_4$
Tobermorite-11	$Ca_5Si_6(OH)O_{16.5}.5H_2O$	$Ca_5Si_6(OH)O_{16.5}\cdot 5H_2O + 10H^+ + 1.5H_2O = 5Ca^{++} + 6H_4SiO_4$
Tobermorite-14	$Ca_5Si_6(OH)O_{16.5}.10H_2O$	$Ca_5Si_6(OH)O_{16.5}\cdot 10H_2O + 10H^+ = 5Ca^{++} + 3.5H_2O + 6H_4SiO_4$
Jennite	$Ca_9Si_6O_{16}(OH)_{10}.6(H_2O)$	$Ca_9Si_6O_{16}(OH)_{10}\cdot 6(H_2O) + 18H^+ = 9Ca^{++} + 8H_2O + 6H_4SiO_4$
Xonotlite	$Ca_6Si_6O_{17}(OH)_2$	$Ca_6Si_6O_{17}(OH)_2 + 12H^+ + 5H_2O = 6Ca^{++} + 6H_4SiO_4$
Foshagite	$Ca_4Si_3O_9(OH)_2.0.5H2O$	$Ca_4Si_3O_9(OH)_2\cdot 0.5H_2O + 8H^+ + 0.5H_2O = 4Ca^{++} + 3H_4SiO_4$
Afwillite	$Ca_3Si_2O_6(OH)_2.2H_2O$	$Ca_3Si_2O_6(OH)_2\cdot 2H_2O + 6H^+ = 3Ca^{++} + 2H_2O + 2H_4SiO_4$
Hillebrandite	$Ca_2SiO_3(OH)_2.0.17H_2O$	$Ca_2SiO_3(OH)_2\cdot 0.17H_2O + 4H^+ = 2Ca^{++} + 1.17H_2O + H_4SiO_4$
Truscottite	$Ca_7Si_{12}O_{29}(OH)_4.H_2O$	$Ca_7Si_{12}O_{29}(OH)_4\cdot H_2O + 14H^+ + 14H_2O = 7Ca^{++} + 12H_4SiO_4$
C2SH,α	$Ca_2(HSiO_4)(OH)$	$Ca_2(HSiO_4)(OH) + 4H^+ = 2Ca^{++} + H_2O + H_4SiO_4$
Jaffeite	$Ca_6(Si_2O_7)(OH)_6$	$Ca_6(Si_2O_7)(OH)_6 + 12H^+ = 6Ca^{++} + 5H_2O + 2H_4SiO_4$
Nanocrystalline C–S–H		
C–S–H1.6	$Ca_{1.6}SiO_{3.6}(OH)_{1.54}.1.81H_2O$	$Ca_{1.6}SiO_{3.6}(OH)_{1.54}\cdot 1.81H_2O + 3.2H^+ = 1.6Ca^{++} + 2.18H_2O + H_4SiO_4$
C–S–H1.2	$Ca_{1.2}SiO_{3.2}(OH)_{1.08}.1.52H_2O$	$Ca_{1.2}SiO_{3.2}(OH)_{1.08}\cdot 1.52H_2O + 2.4H^+ = 1.2Ca^{++} + 1.26H_2O + H_4SiO_4$
C–S–H0.8	$Ca_{0.8}SiO_{2.8}(OH)_{0.6}.1.24H_2O$	$Ca_{0.8}SiO_{2.8}(OH)_{0.6}\cdot 1.24H_2O + 1.6H^+ = 0.8Ca^{++} + 0.34H_2O + H_4SiO_4$
Other		
Portlandite	$Ca(OH)_2$	$Ca(OH)_2 + 2H^+ = Ca^{++} + 2H_2O$

considered C–S–H as a discrete CaH_2SiO_4 phase, but which had variable solubility properties as a function of C/S ratio. Solid solutions may be integrated in most of the geochemical codes. The major disadvantage is an increase in the computation time, or even the appearance of instabilities, particularly for reactive transport codes. On the other hand, the existence of C–S–H with C/S ratio within narrow ranges of values has been widely investigated [15,46–49]. Some structural studies indicate that at least three types of C–S–H with different C/S ratios and polymerization degrees may be observed at room temperature. For low concentrations in dissolved calcium, Grutzeck et al. [48] observe two distinct phases, based on ^{29}Si NMR (Nuclear Magnetic Resonance) analyses. One phase would have a C/S ratio ranging from 0.65 to 1.0 and the other one from 1.0 to 1.3. When higher concentrations in dissolved calcium are reached, Taylor [50] supports the existence of a third phase with a C/S ratio slightly below 2 and a structure close to that of jennite. In addition, Taylor [50,51] confirm the existence of a C–S–H with a C/S ratio close to 1.1 and a crystalline structure similar to that of tobermorite. According to these mineralogical evidences, Stronach and Glasser [52] and Courault [15] have developed a solubility model based on three phases with fixed C/S ratio:

- C–S–H0.8, C/S = 0.8
- C–S–H1.1, C/S = 1.1
- C–S–H1.8, C/S = 1.8.

Following these authors, we have retained a 3-phase model, consistent with the review of Bourbon et al. [5]. Lacking for an overall agreement on C–S–H compositions, we have also calculated the C/S ratios of these phases from solid and solution analyses collected in the literature.

3.1.2. Determined C/S ratio of nanocrystalline C–S–H phases

In order to estimate the composition and the solubility of the three C–S–H phases, we have collected a set of experimental works that provide the composition of the solution and the C/S ratio of solids. The collected data are displayed in Figs. 1–3.

It may be observed that the dispersion of the data is very high. We have investigated the influence of temperature on solution compositions. Indeed, the equilibrium temperatures vary between 30 °C [46,53,54], 25 °C [15,47,55] or 17 °C [50]. If one considers Fig. 1, it may be observed that, between 10 and 15 mmol/l, the distribution of C/S ratios in the solid falls between the values of Flint and Wells [46] and those of Roller and Erwin [53], two sets of data acquired at the same temperature, 30 °C. Thus, temperature does not appear to play the major role in the dispersion of the values. Other parameters may consequently be invoked, such as:

- the synthesis process [43],
- carbonation that may lead to the precipitation of calcite ($CaCO_3$), which changes the C/S in the solid and also changes pH [125]
- the pathway followed to reach equilibrium (dissolution or precipitation) [46] and the reaction time,
- the assessment of the C/S ratio from the initial C/S ratio, as shown by Courault [15]. It should be pointed out that the C/S ratios provided in Courault [15] study correspond to actual microprobe analyses.

In Fig. 1, the *y*-axis corresponds to the C/S ratio in the solid and the *x*-axis represents the dissolved calcium concentration. In order to determine the C/S ratio of the 3 C–S–H phases and the corresponding composition of aqueous solutions, we used a least squares algorithm against experimental data. The results are displayed in Figs. 1–3 and on Table 3. Finally, the following C–S–H compositions are obtained:

- C/S = 1.6 ± 0.10
- C/S = 1.2 ± 0.18
- C/S = 0.8 ± 0.16.

The two latter values are close to the values retained by Stronach and Glasser [52] and Courault [15]. On the other hand, the first one is relatively poor in calcium compared to the values reported by these authors, but it is similar to the value 1.7 determined by Atkins et al. [56].

3.1.3. Equilibrium constants for nanocrystalline C–S–H phases

Equilibrium constants are calculated from aqueous solutions compositions obtained during the previous step. Results are displayed in Table 3.

In Table 3, the columns termed “regression” correspond to the compositions previously determined. These compositions were established from geometric constraints without geochemical considerations. We have used these compositions as first entries in order to model each equilibrium with the PHREEQC code [27] and the database described previously. Equilibrium constants were then adjusted so as to reduce the discrepancy with Table 3 solution compositions. The difference between previously calculated and regressed solution compositions are reported in Table 3 and in Figs. 1–3. Discrepancies are limited, excepted for dissolved calcium concentration in the CSH1.6/CSH1.2 equilibrium case.

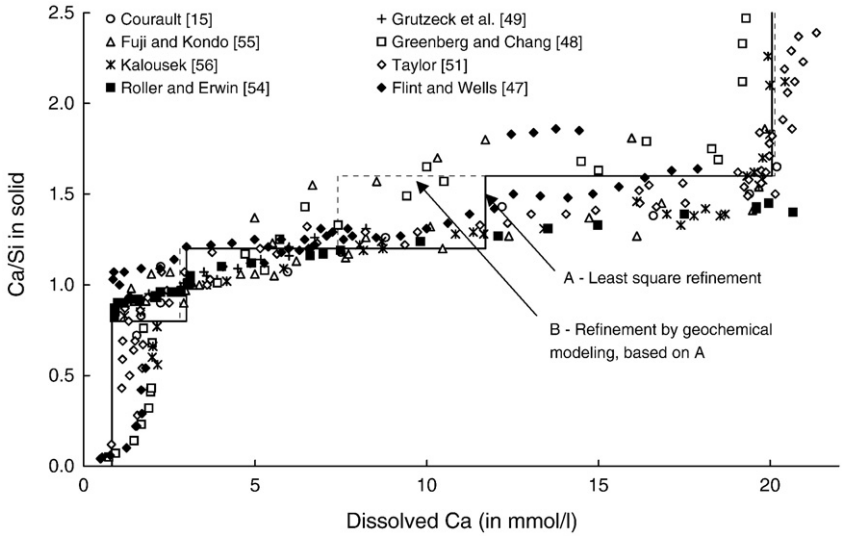

Fig. 1. Relation between C/S in C–S–H and dissolved calcium concentration, according to different authors.

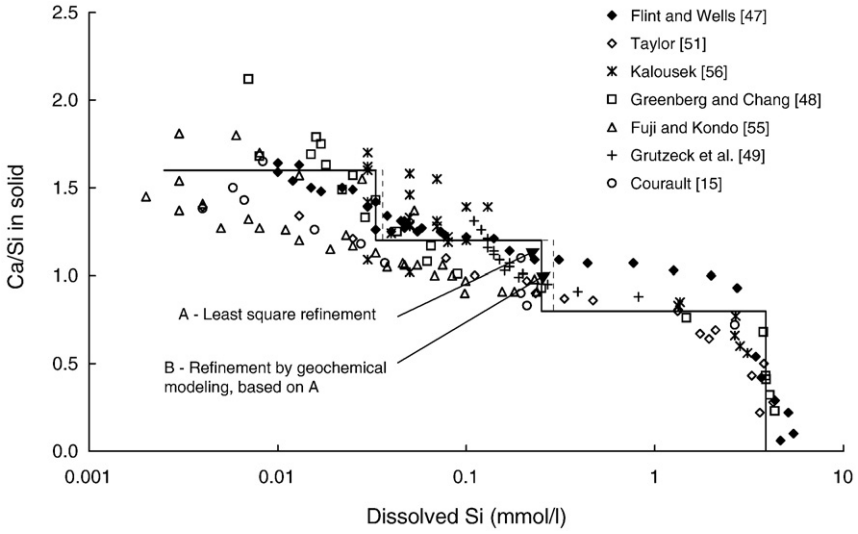

Fig. 2. Relation between C/S in C–S–H and dissolved silica concentration, according to different authors.

Even then, they don't exceed the scattering of the experimental points. The following equilibrium constants are obtained:

- CSH1.6: Log$K$ = 28.00
- CS–H1.2: Log$K$ = 19.30
- CSH 0.8: Log$K$ = 11.05
- Portlandite: Log$K$ = 22.81

The latter value is identical to the 22.81 ± 0.4 value provided by Reardon [57] and Glasser et al. [14] and it is also close to the value of 22.80 found by Humel et al. [30] and Nordstrom et al. [58].

It is more difficult to compare Log$K$ values for C–S–H phase since the retained C/S ratio may differ according to the authors. In addition, Log$K$ value may extends over nearly 20 log units. Simply representing Log$K$ as a function of C/S would thus eliminate any difference. To overcome this effect, we have established a relation between the Log$K$ from this study and C/S ratio:

$$\mathrm{Log}K(C/S) = -1.41*(C/S)^2 - 17.81*C/S + 4.10 \quad (8)$$

Then, we have displayed, in Fig. 4, the difference between the values collected in the literature and those provided through relation (8). The results stemming from this work are consequently assigned a zero value. It may be observed that the values found lie within all of the literature values. Finally, Fig. 4 may help in providing an estimate of the uncertainty related to our Log$K$ determination, i.e. ± 0.7 log units.

3.1.4. Verification of the proposed model

In order to assess the C–S–H solubility model, we have displayed in Figs. 5 and 6 the functions [Si] = f([Ca]) for each C–S–H composition. It may be noted that the experimental data are spreading out according to three trends that are clearly distinguished when the concentration in dissolved calcium increases and merged when the concentration in dissolved calcium decreases.

These trends correspond globally to the solubility curves calculated for each C–S–H phase (C/S = 0.8, 1.2 and 1.6). It is also worth pointing out that neither the C/S ratios of these C–S–H, nor the values of the solubility constants have been determined by means of this figure. The agreement between experimental points and calculated solubility curves could indicate that C–S–H with C/S ratios close to 0.8 and 1.2 may persist, even for high concentrations in dissolved calcium, and despite the fact that they are metastable compared to CSH1.6.

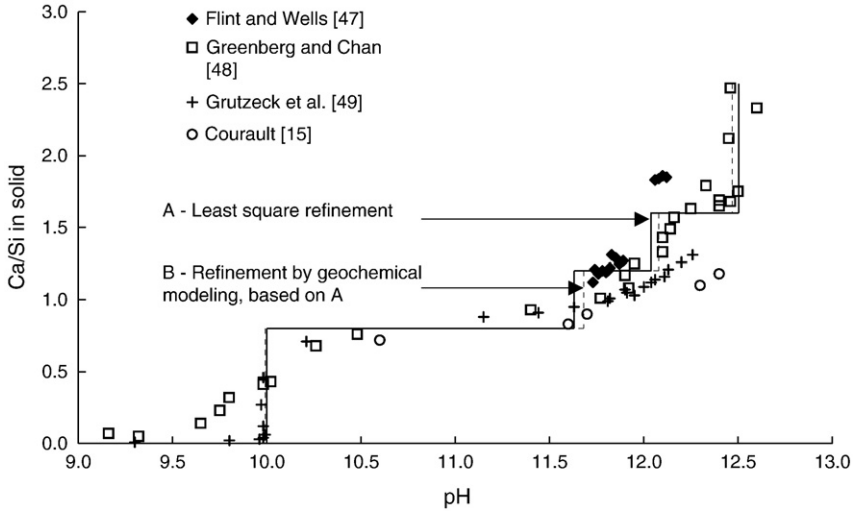

Fig. 3. Relation between C/S in C–S–H and pH, according to different authors.

Table 3
Composition of solutions at equilibrium with C–S–H phases.

Limits	Ca (mmol l^{-1})		Si (mmol l^{-1})		pH	
References	[15,46–48,50,53–55]		[15,46–48,50,54,55]		[47,49,55,56]	
	Regression[a]	PHREEQC[b]	Regression	PHREEQC	Regression	PHREEQC
Portlandite/CSH1.6	20.06	20.14	$2.50 \cdot 10^{-3}$	$2.30 \cdot 10^{-3}$	12.50	12.47
C–S–H1.6/C–S–H1.2	11.71	7.40	0.033	0.036	12.04	12.08
C–S–H1.2/C–S–H0.8	3.00	2.80	0.250	0.290	11.63	11.68

[a] Least square minimization.
[b] From geochemical modeling, based on compositions[a].

Such alignments have already been highlighted by Chen et al. [43], who have even distinguished four curves instead of three.

In Fig. 5, we have also shown the solubility curve of an ideal solid solution, with end members composition C/S = 1.6 and C/S = 0.8. Compared to the experimental points, an improvement of the calculated curve location is observed, as the dissolved calcium falls close to 7 mmol/l. Nevertheless, it clearly appears that, in order to perfectly match the experimental point distribution, the stabilization energy of the solid solution should be higher, implying a regular ordering between both end members [59]. However, the MAS NMR analyses carried out by Grutzeck et al. [48] do not indicate such an ordering.

Besides, it is possible that a solid with variable composition keeps its composition constant despite variations in the composition of the aqueous solution. Glynn and Reardon [60] largely discussed such a specific metastable "stoichiometric saturation" equilibrium state. The relation derived by these authors allows predicting the composition of the aqueous solution at equilibrium with a solid phase of variable composition (binary). However, to our knowledge, no relation allows yet to predict the composition of the precipitated solid [60] at stoichiometric saturation. It should also be pointed out that this metastable state can last. Indeed, among the data from Grutzeck et al. [48], part of these is aligned following the CSH0.8 solubility curve, in spite of a two year equilibration time. On the other hand, it should be noted that the experiments of Roller and Erwin [53] lasted 5 days, to the most. However, the results of these authors are aligned, from 7 to 20 mmol/l, along the CSH1.2 solubility curve. This means that the two years Grutzeck et al. [48] experiments lead to more soluble solid phases than the 5 days experiments of Roller and Erwin [53]. The reaction time is therefore not the only factor responsible for the equilibrium state.

Stronach and Glasser [52] have proposed a three C–S–H solubility model, based on Ca/Si ratio 1.8, 1.1 and 0.8. Given the equilibrium constants refined from these authors, ones obtain the CSH1.8/1.1 at [Ca++] = 18.1 mMol/l. If we consider the equilibrium constant published more recently by Glasser et al. [14], the same equilibrium provides a dissolved calcium concentration of 14.9 mMol/l. This is still far from the 7 mMol/l we have found here for the CSH1.6/1.2 transition but it implies a variation, even considering the same Ca/Si ratio and the same group of authors. Atkins et al. [56] have considered some slightly different Ca/Si ratio 1.7, 1.3 and 0.9. We could calculate that the CSH1.3/0.9 equilibria occurs for a dissolved calcium concentration of 9.5 mMol/l. This is an example of a solubility model implying an invariant point close to that we obtained. From a large collection of experimental data, Chen et al. [43] have proposed a [Si] = f[Ca] graph displaying several trends. They obtained namely 3 curves C″, C′ and C, instead of 2 in our case, and in addition to the curve corresponding to the minimum solubility (A). Curve C″ departs from curve (A) for a calcium concentration close to 7 mMol/l. The authors indicate that curves C″, C′ and C may correspond to metastable equilibria, which does agree with our hypothesis. But they also indicate that in experiments Ca/Si ratio may vary along C″, C′ and C curves. Finally it appears that the calcium concentration at invariant point depends on the Ca/Si ratio and equilibrium constants considered, that results similar to ours have already been obtained previously but the comparison with experimental results indicates that an additional degree of complexity may be involved.

In Fig. 6, the limits obtained previously are compared to those defined from experimental data by Jennings [10]. This author defines two M and S curves between the solubility limits of amorphous silica and portlandite. The S curve is close to the one resulting from the solubility of the three CSH1.6, 1.2 and 0.8. It merges with the solubility of the ideal solid solution. The S curve thus corresponds to the minimum solubility for C–S–H, corresponding to the thermodynamic equilibrium. This interpretation is similar to the conclusions of Jennings [10]. On the other hand, the M curve remains unexplained,

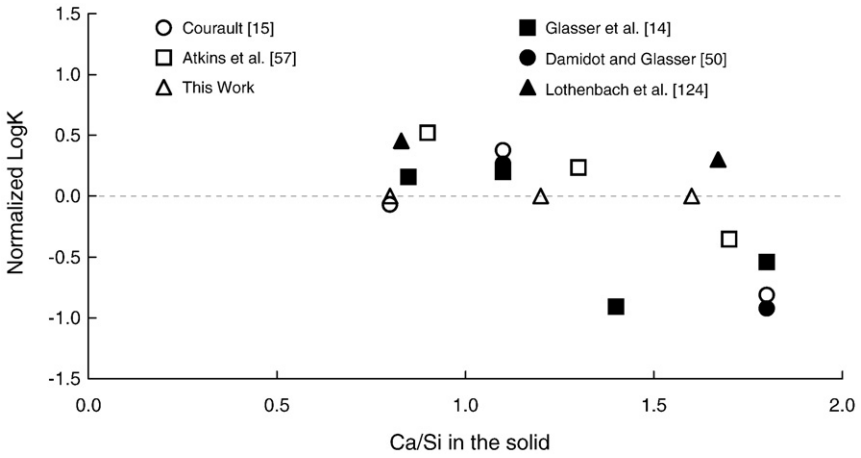

Fig. 4. Comparison between equilibrium constants calculated in this work with literature data.

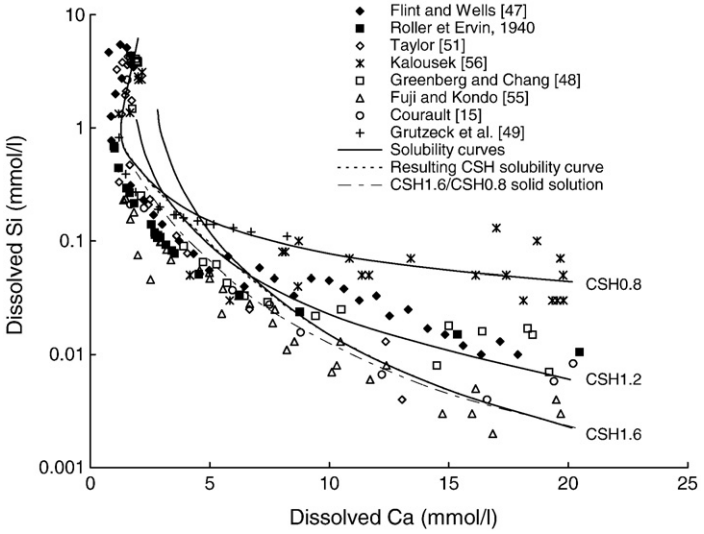

Fig. 5. Composition of the solutions at equilibrium with nanocystalline C–S–H.

especially for low dissolved calcium concentrations. For Chen et al. [43], it should only concern the experiments carried out with short reaction times and C_3S and C_2S as solid precursors. It would result from a metastable hydrate phase covering the surface of C_3S and C_2S grains.

Chen et al. [43] indicate a relation between the method of preparation of the C–S–H and their solubility. For instance, the products prepared from sodium metasilicate (Na_2SiO_3) and calcium nitrate ($Ca(NO_3)_2$) would be at equilibrium with the solutions located next to the S curve [50,53,54].

In addition, those synthesis processes can produce sodium impurities that may also influence thermodynamic equilibria. We have tried here to assess the displacement of the solubility curve produced by the addition of such impurities. Roller and Erwin [53] indicate that their C–S–H, prepared by means of this method, contains 0.05% of Na_2O. We have displayed in Fig. 6, a curve represented by white squares. It corresponds to the minimum solubility of the three CSH1.6, 1.2 and 0.8 phases, equilibrated with a solution containing NaOH 5 mmol/l. This curve is almost overlapping the S curve of Jennings [10]. It then falls closest to the experimental compositions for dissolved Ca <5 mmol/l than the curve calculated by equilibrating C–S–H phases in pure water only (white circles). This calculation therefore indicates that the presence of Na_2O impurities in the equilibrated solution could explain, by itself, the slight discrepancy between our model and the S curve, for dissolved Ca <5 mmol/l. Indeed, if 100 g of C–S–H with 0.05% Na_2O are placed in a 1 l recipient and the dissolution of Na_2O is complete, the resulting solution contains 1.7 mmol/l in dissolved sodium. Unfortunately, the details provided by the authors are not sufficient to calculate precisely this concentration.

In conclusion, the method based on sodium metasilicate, which enables a quick C–S–H dissolution, produces solutions located along the S curve, according to Chen et al. [43]. In addition, sodium impurities produces an uncertainty for the location of minimum solubility curves that strongly interfere and prevent a clear discussion

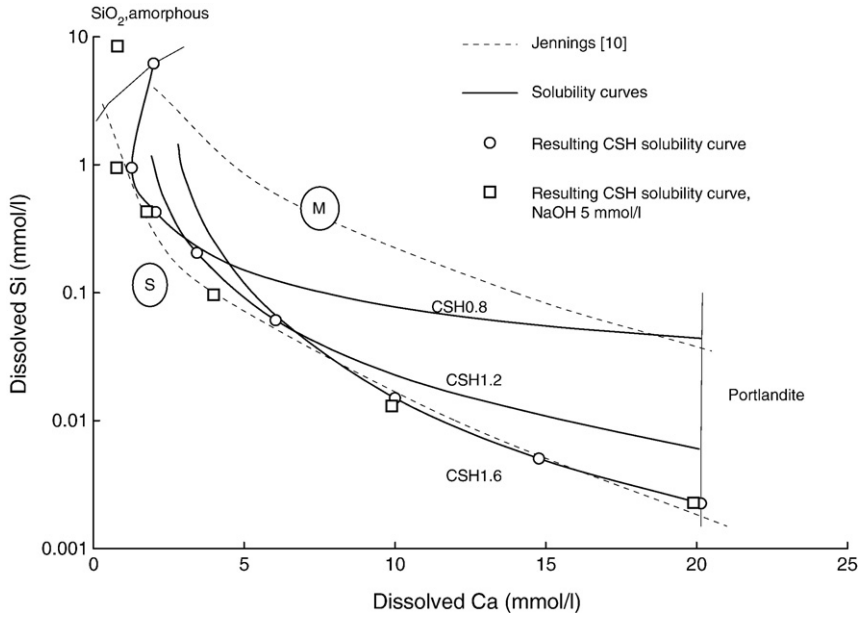

Fig. 6. Phase relations in the system $CaO–SiO_2–H_2O$ at 25 °C, modified from Jennings [10].

about C–S–H solubility models, either based on discrete or continuous composition phases. Last, the metastable equilibrium states highlighted in this study should be taken into account in such a discussion, as well as for selecting C–S–H solubility experimental dataset.

3.2. Crystalline C–S–H phases

The following paragraph is devoted to crystalline C–S–H phases. These phases may be of importance for the long term modeling of cementitious materials in storage context [61]. In addition, the determination of their thermodynamic properties will enable us to develop a method for estimating the thermodynamic properties of nanocrystalline C–S–H.

3.2.1. Stable phases

Different experiments had already been carried out concerning the stability field of crystalline C–S–H but a coherent picture does not emerge, yet. From this point of view, it is required, first to determine the thermodynamically stable phases from the metastable ones, as this point remains often unclear [63–66]. This section is devoted to this specific issue.

The name and the structural formula of the main crystalline C–S–H are reported in Table 2. The criteria for reaching thermodynamic equilibrium have been discussed by different authors [60,62]. For phases of discrete composition, those criteria correspond to:

- The independence of the final assemblage with respect to the reaction pathway, the nature of the reagents and time.
- The reversibility of the phenomena.

Many crystalline C–S–H seem to represent transitory states with respect to strict thermodynamic equilibrium:

- the Z phase, C9S6H, determined by Assarsson [64] could be a transitory step towards gyrolite after Jauberthie et al. [65]
- the Y phase or dellaite, C6S3H, discovered by Roy [63], represents a metastable precursor for jaffeite and kilchoanite, after the work of Yanagisawa [66]
- the C2SH,α and C2SH,γ phases obtained by Assarsson [64] are considered as metastable, with respect to hillebrandite [67] for the α phase and compared to jaffeite [66] or kilchoanite [68] for the γ phase.
- kilchoanite, C8S5, has been determined by Ahmed and Taylor [68], who demonstrated its metastability compared to hillebrandite or foshagite at 180 and 250 °C.
- calcio-chondrite or reinhardbraunsite, C5S2H, is described by Harker [62] and Ahmed and Taylor [68] and is found to be metastable with respect to hillebrandite at 180 and 250 °C [68]
- the F phase, C5S3H2, is obtained by Aitken and Taylor [69], and is shown to be metastable by the same authors, with respect to xonotlite, at 165 °C
- the K phase, C7S16H, analyzed by Gard et al. [70] is considered by the same authors as metastable compared to truscottite.

Field observations are also of use in order to determine the stable character of C–S–H phases. In that case, the equilibration time represents hundreds of thousands of years whereas, in most cases, equilibration experiments last around several weeks or months. It may consequently be assumed that the minerals observed in natural contexts correspond to thermodynamically stable phases. Those include jennite and tobermorite [71], observed as fracture infilling on several samples from the Maqarin site (Jordan). This is also the case for jennite and afwillite, which appear as fracture infilling in the Fuka skarn zone (Okayama prefecture, Japan, [72]). In this latter case, jennite seems to have precipitated at lower temperature, probably from the alteration of afwillite. Moreover, gyrolite and okenite are usually found associated with low temperature zeolites like apophyllite [73], itself related to chabazite [74]. Chabazite precipitates at temperatures ranging between 0 and 135 °C, according to Rançon [75]. These observations would restrain gyrolite and okenite to low temperature domains. Xonotlite is observed associated with natrolite [76]. According to Rançon [75], this would imply a temperature of formation ranging between 100 and 250 °C. Similarly, Bargar et al. [79] have identified truscottite related to laumontite, which requires a higher formation temperature between 180 and 300 °C [75]. Concerning Hillebrandite and foshagite, these minerals have been observed in natural samples of the Bushveld skarn formation by Buick et al. [77]. Jaffeite (C6S2H3) has finally been determined in some Namibian samples by Sarp and Peacor [78].

In conclusion, we can consider as thermodynamically stable the following minerals: jaffeite, hillebrandite, afwillite, jennite, xonotlite, foshagite, tobermorite, gyrolite and okenite. Among these, afwillite, jennite, gyrolite and okenite should be restricted to low temperature domains.

3.2.2. Thermodynamic data and phase relations

Few calorimetric measurements are available to date for C–S–H. Thus, estimates from Babushkin et al. [80] are widely used. However, the enthalpies of formation of hillebrandite, xonotlite and foshagite have been measured by Newman [81] (34.7, 94.6 and 92.6 kcal/mol respectively), who obtained data related to the constituent oxides. We have retained the theoretical compositions provided by Babushkin et al. [80], which differ slightly from those used by Newman [81]. In order to take into account those measurements, we have to consider a theoretical conversion reaction, i.e. for xonotlite:

$$\underset{\text{xonotlite, Newman [83]}}{5CaO{\cdot}5SiO_2 : H_2O} + SiO_2 + CaO \leftrightarrow \underset{\text{xonotlite, Babushkinetal. [82]}}{6CaO{\cdot}6SiO_2 : H_2O} \quad (9)$$

Given the formation enthalpy of the constituents:

- $\Delta_f H^0_{Pr,Tr}$ (SiO_2,quartz), −910.70 kJ/mol [18],
- $\Delta_f H^0_{Pr,Tr}$ (CaO, lime), −634.92 kJ/mol [82],
- $\Delta_f H^0_{Pr,Tr}$ (H_2O), −285.83 kJ/mol [18],

Babushkin's xonotlite $\Delta_f H^0_{Pr,Tr}$ may then be calculated from reaction (9). The process is extended to hillebrandite and foshagite. The results are given in Table 4 and compared to Babushkin et al.'s [80] estimates. For the three phases, the main difference is close to 6 kJ/mol, which is rather low for minerals of such high molecular weight. For tobermorite-11 , Savage et al. [83] collected the enthalpies of formation available throughout the literature. These authors report a high dispersion of values. The measurements from Zuern and Fehr [84] fall rather close to Babushkin et al. [80] results. The results of Taylor [85], differ significantly from the whole dataset, which could be explained by the aluminum amount included into the composition of the natural phase considered. We finally have retained the value provided by Zuern and Fehr [84].

From Babushkin et al. [80] estimates (Table 4), we have plotted the stability diagram of the C–S–H as a function of temperature in Fig. 7. Some inconsistencies arise with respect to previous studies. First, the transition between tobermorite-11 and tobermorite-14 occurs at 86 °C whereas, according to Maeshima et al. [86], it should take place at 105 °C. In addition, gyrolite remains stable only over a rather limited temperature interval, between 60 and 140 °C, whereas most of the authors obtained this phase from the ambient up to 200 °C [69,87,88]. The stability field of foshagite extends over all the temperature, whereas it is generally accepted as a high temperature phase [88], the lowest formation temperature, 130 °C, being obtained by Hong and Glasser [89]. Okenite and afwillite appear to be metastable, in disagreement with the preceding literature review. From Fig. 7, xonotlite begins to form at 200 °C, whereas the transition between this phase and tobermorite is obtained by El-Hemaly et al.

Table 4
Literature review of the available thermodynamic properties of crystalline C–S–H.

Mineral	$\Delta_f G^0_{Pr,Tr}$ (kJ mol^{-1})	$\Delta_f H^0_{Pr,Tr}$ (kJ mol^{-1})		$S^0_{Pr,Tr}$ (J mol^{-1} K^{-1})	Cp(298) (J mol^{-1} K^{-1})
	[80]	[80]	Other	[80]	[80]
Okenite	−2871.90	−3139.26		171.13	187.48
Gyrolite	−4542.36	−4919.76		267.78	295.18
Tobermorite-11	−9880.31	−10,695.56	−10,680.92 [84]	611.49	698.52
Tobermorite-14	−11,076.30	−12,180.67		808.14	889.94
Xonotlite	−9453.33	−10,027.79	−10,022.15 [80]	507.52	548.30
Foshagite	−5639.61	−6024.54	−6032.43 [80]	330.33	309.46
Afwillite	−4405.54	−4783.15		312.32	328.38
Hillebrandite	−2480.69	−2665.84	−2662.48 [80]	160.67	166.63
Portlandite			−984.55	83.39	87.49

(1) $S^0_{Pr,Tr}$ from Chase [83], $\Delta_f H^0_{Pr,Tr}$ from combining $S^0_{Pr,Tr}$ and the equilibrium constant Log$K$ = 22.81 calculated in this study, Cp(298) from Akinfiev and Zotov [99].

[90] from 140 °C. All of these points lead us to propose a refinement of the C–S–H stability diagram.

3.2.3. Refinement of the phase diagram

3.2.3.1. Constraints and calculation process. From what precedes, we are already able to propose a measured value for the formation enthalpy of tobermorite-11A, xonotlite, hillebrandite and foshagite. Additional constraints are provided by:

- an assessment of the equilibrium temperature for ternary assemblages in the CaO–SiO_2–H_2O system
- equilibrium constants
- estimation methods

Indeed, the Gibbs phase rule indicates that in the system CaO–SiO_2–H_2O at variable temperature, a ternary assemblage consists in an invariable point. In that case, the free enthalpy of the equilibrium reaction equals to zero, which allows performing thermodynamic calculations. Similar methods had already been used in a metamorphic context, by Berman [91] and Holland and Powell [92], for example.

The constraints that we have been able to identify are reported in Table 5 with given mineral assemblages associated with temperatures. The temperatures actually obtained after minimization are given in brackets.

For the afwillite–hillebrandite–portlandite assemblage, Hong and Glasser [89] and Heller and Taylor [93] indicate an equilibrium temperature of 130 and 140 °C, respectively. However, if the C2SH,α, a phase of same composition, is considered as metastable compared to hillebrandite as emphasized by Hu et al. [67], the temperature at which this assemblage appears must be decreased. The lowest temperature is an estimate provided by Atkinson et al. [94], 100 °C, which we have adopted. The temperature of the tobermorite-11 –xonotlite–gyrolite assemblage is given directly by Kalousek and Nelson [95], i.e. 175 °C. In addition, tobermorite-11 and xonotlite could form a stable assemblage with a phase having a C/S higher than 1. The equilibrium temperature could be close to 140 °C, the temperature found by El-Hemaly et al. [90] for the tobermorite-11 –xonotlite transition. For Hong and Glasser [89], xonotlite should be replaced by foshagite but no other work has reported such a low temperature for the appearance of foshagite. Hong and Glasser [89] have determined for the foshagite–hillebrandite–afwillite assemblage a temperature of 170 °C by assuming, namely, that jennite is metastable. An additional ternary assemblage is proposed both by Hong and Glasser [89] and Atkinson et al. [94]. Actually, the two groups of authors propose, for the afwillite–hillebrandite–xonotlite assemblage, a tentative temperature of 150 °C. It should be noted that the temperature is obtained only by construction. The tobermorite–14 /tobermorite–11 transition temperature has been determined by Maeshima et al. [86], i.e. 105 °C. Finally, the relation between jennite and afwillite still needs to be elucidated. Kusachi et al. [72] have shown that both may exhibit their own stability field and that the low temperature phase should be jennite. To determine the transition temperature, we have considered the work of Atkins et al. [41]. These authors observed at 55 °C, that the phase transition took place between 13 and 26 weeks of reaction. The actual transition temperature should be lower but, in first approximation, we have selected this value.

In Table 5 are shown two other groups of constraints. First, the solutions equilibrated by Atkins et al. [41] have enabled to calculate the 85 °C equilibrium constant of tobermorite-14 . In addition, Revertegat et al. [96] experimentally obtained two values that allow us to frame the equilibrium constant of jennite. Jaffeite, truscottite and okenite were discarded from the calibration dataset because of a lack of estimates from Babushkin et al. [80] or of references for verification.

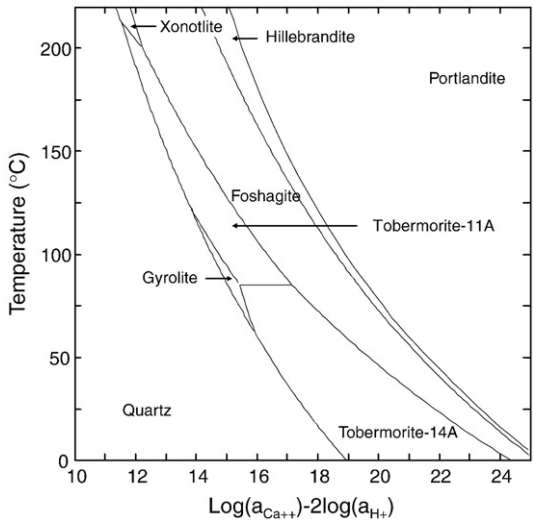

Fig. 7. Phase diagram in the CaO–SiO_2–H_2O system, using thermodynamic properties estimated by Babushkin et al. [80].

Table 5
Constraints used for refining the thermodynamic constants of crystalline C–S–H phases.

Phases	Equilibrium temperature (°C)	References
AFW + POR + HIL	100 (100)	[89,93]
AFW + FOS + HIL	170 (169)	[89]
AFW + XON + HIL	150 (150)	[89,94]
TOB11 + AFW + XON	140 (140)	[91]
TOB11 + TOB14	105 (104)	[86]
TOB11 + XON + GYR	175 (174)	[95]
JEN + AFW	T < 55 °C (55)	[41]
Tobermorite-14 : Log$K_{85°C}$ = 54.25 (54.25)		[41]
Jennite: 147.10 < Log$K_{25\ °C}$ < 150.81 (147.33)		[96]

In parentheses: results obtained after the refinement process.

In order to decrease the number of unknowns we have calculated a linear relation between Babushkin et al. [80] estimates of S° and Cp (298), with $R^2 = 0.993$.

3.2.3.2. C–S–H phase diagram refinement: results. The results of the calculation are given in Tables 6 and 10, and are also reported in Fig. 8. The latter indicates that jennite, tobermorite-14A, hillebrandite and gyrolite are stable at 25 °C. As the temperature increases, gyrolite and hillebrandite remain stable and afwillite, tobermorite-11A then xonotlite appear successively. It is interesting to verify that jennite can actually be a part of the thermodynamically stable phases in the $CaO–SiO_2–H_2O$ system. This point was not obvious before this calculation since our only temperature constraint for jennite consists of an inequality. On the other hand, foshagite disappears from the list of stable minerals. It is possible that 170 °C for the afwillite–hillebrandite–foshagite assemblage is a somewhat low temperature; Speakman [88], for example, have obtained foshagite only from 259 °C.

The diagram in Fig. 8 has to be read by keeping some warnings in mind. Because we consider only thermodynamic equilibrium, the stability fields of transition phases have not been taken into account. The diagram thereby obtained is more representative of the state of the system after a long period of time. However, it represents an improvement, allowing namely to precise phase relations between jennite and afwillite.

In Table 6 we have compared the equilibrium constants at 25 °C obtained in this work with the values calculated using the estimates of Babushkin et al. [80] and with the experimental values provided by Dickson et al. [13]. Globally, we have obtained values close to those calculated from the estimates of Babushkin et al. [80]. On the other hand, even if our results fall within the interval defined by Dickson et al. [13] for gyrolite and tobermorite-11 , this is not the case for the other phases. It seems that Dickson et al. [13] aimed to equilibrate phases that could not be at equilibrium at 25 °C. This could even explain the large interval of values obtained by Dickson et al. [13], in particular for the equilibrium constant of afwillite. For this latter phase, our results are in disagreement with the values of Babushkin et al. [80]. On the other hand, they are intermediate between the results of these authors and those of Dickson et al. [13]. In addition, the set of thermodynamic data calculated in this work enables an effective stability field to be defined for this phase whereas the values of Babushkin et al. [80] imply a solubility so high that afwillite completely disappears from the phase diagram (Fig. 7). In addition, the presence of foreign chemical elements in Dickson et al. [13] mineral phases, such as aluminum, may lead to the extension of the stability field of tobermorite [90,97,98].

The uncertainty relative to the calculations performed in this work is difficult to estimate, concerning a minimization performed under constraints and including inequalities. A comparison with the values of Babushkin et al. [80] and Newman [81] makes it possible to broadly evaluate at ±1 the uncertainty in logK, i.e. close to ±5 kJ/mol for the enthalpies and free enthalpies of formation and ±15 J/mol K for the entropy. These numbers are only given there as indicative values and do not rely on a statistical determination.

Table 6
Comparison of crystalline C–S–H equilibrium constants, at 25 °C, either from the literature or obtained after the refinement of the phase diagram.

Mineral	Babushkin et al. [80]	Dickson et al. [13]	This study
Okenite	9.90	5.01	
Gyrolite	24.20	17.88 to 22.82	22.34
Tobermorite-11	67.25	62.42 to 70.05	65.58
Tobermorite-14	65.44		62.94
Xonotlite	93.81	66.49	91.34
Foshagite	65.50	57.33 to 60.12	65.96
Afwillite	60.63	40.58 to 46.51	49.42
Hillebrandite	37.26	32.18	36.85

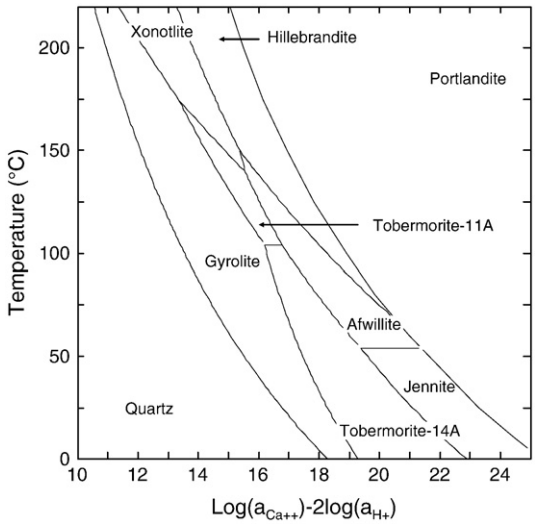

Fig. 8. Phase diagram in the $CaO–SiO_2–H_2O$ system, thermodynamic properties refined in this work.

4. Development of a polyhedral model to complete the properties of nanocrystalline C–S–H and associated phases

The investigation of C–S–H stability up to 100 °C, however, requires calculating the dependency of the equilibrium constant with temperature. This implies to assess the formation enthalpy and heat capacity, since those properties are not available directly in the literature, which is performed here by using a polyhedral decomposition method [100–102]. This method is derived from the conventional oxide summation method [103,104]. Compared to Helgeson et al.'s [27] method based on fictive solid–solid reactions, it relies on a large set of calibration minerals but it may be extended to all thermodynamic properties of minerals, as has been shown by La Iglesia and Felix [102]. Following the approach of La Iglesia and Felix [102], we have extended the calculations to $\Delta_f G^0_{Pr,Tr}$, $\Delta_f H^0_{Pr,Tr}$, Cp(298) and V^0.

4.1. Chemical system, calibration mineral set and polyhedral units

Polyhedral decomposition is thus applied to the system $SiO_2–CaO–H_2O$. In this system, we have selected 11 minerals, whose thermodynamic properties had been refined previously: CSH1.6, 1.2, and 0.8, tobermorite-11A and 14A, jennite, xonotlite, hillebrandite, foshagite, gyrolite and afwillite. For $\Delta_f G^0_{Pr,Tr}$ and V^0 estimate, the calibration dataset comprises the 11 phases but, as $\Delta_f H^0_{Pr,Tr}$ and Cp(298) are unknown for nanocrystalline C–S–H, this number is reduced to 8 for those two latter parameters.

For the polyhedral units (base units), we have considered, for calcium and silicon, oxide and hydroxide groups, i.e.: CaO^{Vi}, $Ca(OH)_2$, SiO_2^{IV} and $Si(OH)_4^{IV}$, where roman numbers refer to the coordination number of the polyhedron. In addition, we have assumed, from Black et al. [106], that part of the calcium could be hydrated, being linked to the structure through hydrogen bonds (CaO^{int} group). Finally, we have distinguished the molecular water from hydroxyl groups (H_2O group). In our case, it would have been conceivable to associate calcium with molecular water. The splitting enabled to compare the properties of the water with literature data.

The decomposition itself is shown in Table 7. We have calculated the relative proportion of each polyhedral unit, based namely on the recent work of Black et al. [105,106], who determined these proportions by means of XPS (X-ray photoelectron spectroscopy) measurements. This technique enables, in particular, to determine the relative proportions of bridging and non-bridging oxygen within a crystalline structure.

Table 7
Decomposition of C–S–H into constituent oxides and hydroxides.

Mineral	H_2O	CaO^{VI}	CaO^{int}	$Ca(OH)_2^{VI}$	$Si(OH)_4^{IV}$	SiO_2^{IV}
Gyrolite	2.00	1.20	0.30	0.50		3.00
Xonotlite		5.00		1.00		6.00
Tobermorite-14	10.0	3.75	1.25		0.25	5.75
Tobermorite-11	5.00	4.00	1.00		0.25	5.75
Foshagite	0.50	3.00		1.00		3.00
Jennite	6.00	4.00	1.00	4.00	0.50	5.50
Afwillite	2.00	3.00			0.50	1.50
Hillebrandite	0.17	1.00		1.00		1.00
C–S–H1.6	1.81	0.93		0.67	0.05	0.95
C–S–H1.2	1.52	1.08		0.12	0.21	0.79
C–S–H0.8	1.24	0.80			0.15	0.85

CaO^{int} represents the hydrated calcium fraction linked to the structure through hydrogen bounds after Black et al. [105]; roman numbers refer to the coordination number of the polyhedron.

The determination of the relative proportions of hydroxyl groups and molecular water, for the nanocrystalline C–S–H, is based on the ^{29}Si NMR study carried out by Cong et al. [107] on synthesized C–S–H. From the study of Cong et al. [107], we have established a linear relation between the amount of OH groups and the Ca/Si ratio, as follows:

$n_{OH} = 1.16(Ca/Si) - 0.31$, with $R^2 = 0.79$. For the total amount of molecular water, the relation $n_{H2O} = 0.79(Ca/Si) + 0.56$ ($R^2 = 0.83$) has been derived.

4.2. Implementation of the calculation

The polyhedral method supposes that a given calculated property Y is obtained from the sum of the contribution A_j of each basis unit j, for a given mineral i:

$$Y_i = \sum_j A_j \cdot X_{i,j} \quad (10)$$

where $X_{i,j}$ represents the amount of basis unit j for the mineral i.

The A_j terms are obtained by using a least squares algorithm that minimizes the sum of the squared differences $\sum (Y_{obs} - Y_{calc})^2$ between observed Y_{obs} and calculated Y_{calc} values. The minimization over $\Delta_f G^0_{Pr,Tr}$ allows to check the consistency of the decomposition itself, namely for nanocrystalline C–S–H.

4.3. Results

The refined properties of the oxides/hydroxides units are summarized in Table 8 whereas in Table 9 are displayed estimated properties, for each calibration phase, along with the discrepancy with respect to the refined value. In Table 10, those values allow to complete the thermodynamic dataset of a mineral when no other source is available.

Table 8
Properties of the constituent oxides/hydroxides obtained after the polyhedral refinement.

	$\Delta_f G^0_{Pr,Tr}$ (kJ mol^{-1})	$\Delta_f H^0_{Pr,Tr}$ (kJ mol^{-1})	$S^0_{Pr,Tr}$ (J mol^{-1} K^{-1})	Cp(298) (J mol^{-1} K^{-1})	V (cm^3 mol^{-1})
H_2O[a]	−237.87	−298.21	30.86[b]	38.85	12.35
H_2O[c]			40.17	40.03	13.70
H_2O[d]	−269.30	−333.30	42.50	43.10	13.00
CaO^{VI}	−669.72	−699.47		37.12	7.22
CaO^{int}	−693.79	−714.83		46.51	4.30
$Ca(OH)_2^{VI}$	−908.18	−1001.70		33.20	33.76
$Si(OH)_4^{IV}$	−1357.45	−1560.55		39.22	82.50
SiO_2^{IV}	−868.13	−919.64		64.28	30.39

[a] This work.
[b] Calculated in this work by combining $\Delta_f G^0_{Pr,Tr}$ and $\Delta_f H^0_{Pr,Tr}$.
[c] Properties of the structural water defined by Helgeson et al. [28].
[d] Properties of the hydration water for hydroxides and oxihydroxides determined by Mercury et al. [108] (Table 4).

It is interesting to compare the results for the molecular water with some values found in previous works. With respect to the results of Helgeson et al. [28] and Mercury et al. [108], we have obtained a lower value for the entropy, the heat capacity and the molar volume (see Table 8). However, since the uncertainties reported by Mercury et al. [108] on these three parameters are respectively 17 J/mol K, 12.6 J/mol K and 2.1 cm^3/mol, the values calculated here lie within the uncertainty interval. Considering $\Delta_f H^0_{Pr,Tr}$ and $S^0_{Pr,Tr}$, with respect to the classification proposed by Mercury et al. [108], the values refined here correspond to a group of hydratable and hydrophilic minerals [108], (Fig. 4), which is satisfactory given the nature of C–S–H.

In addition, we have estimated the properties of four major phases that were not included in the refinement process. These are truscottite, okenite, jaffeite and the hydrate C2SH,α. The values obtained are reported in Table 10. It may be noted that, compared to the estimates of Babushkin et al. [80] (Table 6), the values found for okenite are rather similar.

4.4. Model verification

4.4.1. Comparison between nanocrystalline phases and crystalline phases

In order to verify the present model, we first have compared, in Fig. 9, the equilibrium constants determined in this study, for both nanocrystalline and crystalline phases. The constants for the truscottite, okenite, jaffeite and C2SH,α are estimated by means of the above mentioned decomposition method. For crystalline phases, equilibrium constants are normalized to the number of Si cations present in the crystallochemical formula.

In this figure, the points representing the nanocrystalline phases are located slightly above, whereas the points representing the crystalline phase are below the main curve. The difference appears rather small with respect to the influence of temperature on equilibrium constants. Indeed, when the curves are closest ($Ca/Si \approx 1$), the difference is 0.43 Log$K$ units, which is not negligible, even if it lies within the uncertainty ranges previously defined either for nanocrystalline or crystalline phases. One can also observe that the curves do not cross, which means that globally, the crystalline phases are more stable than the nanocrystalline ones, as expected.

The values calculated for the $\Delta_f H^0_{Pr,Tr}$ of nanocrystalline C–S–H may be evaluated by mean of the $\Delta_r H^0_{Pr,Tr}$ value. Indeed, it can be calculated from predicted $\Delta_f H^0_{Pr,Tr}$ while experimental values can be deduced from some already published works. Glasser et al. [14,116] have carried out a large study where they namely have measured the solubility of four nanocrystalline C–S–H ($Ca/Si = 1.8, 1.4, 1.1$ and 0.85), at three different temperatures (25, 55 and 85 °C). We have calculated the solubility constants of these phases from solution compositions provided by Glasser et al. [116], by using the PHREEQC software [27] and the aqueous complexes database reported in Table 2. Since we have used the B-dot activity model, we only retained the solutions with an ionic strength of <0.5. At 25 and 55 °C, we have selected the solutions with an ion balance deficit less than 5%. At 85 °C, since no solution could meet this criterion, we have retained the solution with the lowest ion balance deficit. The results are displayed in Fig. 10, as a function of the inverse of temperature. The error bar that widens as the temperature increases corresponds to the standard deviation. The alignment of the points as a function of $1/T$ is relatively good, which allowed us to calculate an enthalpy of reaction, $\Delta_r H^0_{Pr,Tr}$, using the Van't Hoff relation. The latter is an approximation where one supposes that $\Delta_r Cp(298) = 0$. However it can be seen from Fig. 11 that the dispersion of the experimentally derived $\Delta_r H^0_{Pr,Tr}$ is rather large, overcoming the contribution of the heat capacity term. In addition, for each nanocrystalline or crystalline C–S–H phase from Table 2, we have calculated $\Delta_r H^0_{Pr,Tr}$ from $\Delta_f H^0_{Pr,Tr}$ taken either from the literature, from the refinement process or estimated with the polyhedal model when

Table 9
Estimates of the thermodynamic properties of C–S–H phases by the polyhedral model. The Δ column indicates the discrepancy with respect to properties refined from experimental data and reported in Table 10.

Mineral	Estimates							
	$\Delta_f G^0_{Pr,Tr}$ (kJ mol^{-1})	Δ (%)	$\Delta_f H^0_{Pr,Tr}$ (kJ mol^{-1})	Δ (%)	Cp (298) (J mol^{-1} K^{-1})	Δ (%)	V (cm^3 mol^{-1})	Δ (%)
Gyrolite	−4546.02	0.09	−4915.00	0.06	345.62	5.86	142.70	3.83
Xonotlite	−9465.55	0.01	−10,026.87	0.05	604.45	3.92	252.18	1.85
Tobermorite-14	−11,088.48	0.01	−12,176.73	0.01	965.21	0.86	351.30	
Tobermorite-11	−9893.12	0.04	−10,681.83	0.01	768.62	0.48	290.28	1.42
Foshagite	−5640.66	0.05	−6018.12	0.24	356.81	14.24	152.75	5.05
Jennite	−13,886.02	0.01	−15,187.06	0.01	934.01	0.09	450.71	1.26
Afwillite	−4465.81	0.07	−4854.56	0.02	305.07	0.50	133.18	2.78
Hillebrandite	−2486.46	0.18	−2681.50	0.71	141.20	22.76	73.47	1.22
C–S–H1.6	−2554.45	0.14	−2819.79		190.10		84.68	
C–S–H1.2	−2164.72	0.16	−2384.34		162.13		71.95	
C–S–H0.8	−1772.26	0.18	−1945.13		138.38		59.29	

no other option were available. These are compared, in Fig. 11, with reaction enthalpies derived from Glasser et al. [116] experiments. We have also included, in this figure, the reaction enthalpies derived by Courault [15], from equilibrium experiments carried out at 25 and 85 °C, for two nanocrystalline phases (Ca/Si = 0.8 and 1.1). For the crystalline phases, reaction enthalpies are normalized to the number of Si cations in the crystallochemical formula. I

It may be observed that the experimental values for nanocrystalline C–S–H are a little more scattered than for crystalline phases. However, the values estimated in this work for the nanocrystalline phases are in agreement with the experimental values. The points representing nanocrystalline phases are located above the points standing for crystalline phase. It is possible to compare this, for example, with the thermodynamical status of the different gibbsite minerals. The $\Delta_r H^0_{Pr,Tr}$ collected by Nordstrom et al. [58] actually concern different crystalline states, from the nanocrystalline to the fully crystalline. The values indicate an increase of the reaction enthalpy (but a decrease of the absolute value), as the crystallinity increases. The location of the point representing nanocrystalline and crystalline phases in Fig. 11 is consistent with such a behavior.

4.4.2. Additional minerals in the CaO–SiO$_2$–H$_2$O phase diagram

Finally, it is possible to assess the proposed model by representing the CaO–SiO$_2$–H$_2$O phase diagram, as a function of temperature, including the phases whose thermodynamic properties have been estimated with this model. This diagram is displayed in Fig. 12.

The first interesting point in Fig. 12 is that nanocrystalline C–S–H1.6, 1.2 or 0.8 does not exhibit a proper stability domain even if the temperature may influence their solubility [121]. This is also consistent with the preceding observations concerning phase relations between nanocrystalline and crystalline polymorphs.

We can now consider the stability fields obtained for the phases whose thermodynamic properties have been estimated here.

For okenite, its stability field is limited to a low temperature domain (<50 °C). This result is consistent with the observation, by Cole and Lancucki [122] of this mineral in silicaceous aggregates from a 30 years old Australian dam. This implies a precipitation at room temperature for okenite, consistent with a stability field restricted to low temperature domains. Concerning truscottite, Fig. 12 indicates that it occurs between 135 and 180 °C as a replacement product for gyrolite. This agrees with the results of Harker [62], who has obtained

Table 10
Selected thermodynamic properties of C–S–H phases.

Mineral	Log$K$(298)	$\Delta_f G^0_{Pr,Tr}$ (kJ mol^{-1})	$\Delta_f H^0_{Pr,Tr}$ (kJ mol^{-1})	$S^0_{Pr,Tr}$ (J mol^{-1} K^{-1})	Cp(298) (J mol^{-1} K^{-1})	V (cm^3 mol^{-1})
Crystalline C–S–H						
Gyrolite	22.34	−4550.06	−4917.99^R	309.32^R	325.94^R	137.34$^{(2)}$
Xonotlite	91.34	−9465.12	−10,022.15$^{(10)}$	573.74^R	628.64^R	256.90$^{(3)}$
Tobermorite-14A	62.94	−11,090.12	−12,175.15^R	874.57^R	973.53^R	351.30^P
Tobermorite-11A	65.58	−9889.25	−10,680.92$^{(11)}$	692.55^R	764.91^R	286.19$^{(4)}$
Foshagite	65.96	−5643.83	−6032.43$^{(10)}$	295.07^R	309.38^R	160.66$^{(5)}$
Jennite	147.33	−13,886.77	−15,189.04^R	839.25^R	933.21^R	456.40$^{(1)}$
Afwillite	49.42	−4469.06	−4853.82^R	289.70^R	303.55^R	129.53$^{(6)}$
Hillebrandite	36.95	−2481.95	−2662.48$^{(10)}$	179.71^R	177.46^R	72.58$^{(7)}$
Nanocrystalline C–S–H						
C–S–H1.6	28.00^S	−2550.86	−2819.79^P	154.42	190.10^P	84.68^P
C–S–H1.2	19.30^S	−2161.23	−2384.34^P	129.14	162.13^P	71.95^P
C–S–H0.8	11.05^S	−1769.03	−1945.13^P	107.85	138.38^P	59.29^P
Crystalline C–S–H, properties estimated in this work						
Truscottite	77.08	−15,280.40^P	−16,854.62^P	927.68	1034.10^P	478.73$^{(8)}$
Okenite	9.18	−2881.72^P	−3135.70^P	208.52	210.07^P	94.77$^{(9)}$
C_2SH,α	35.54	−2449.12^P	−2634.92^P	122.38	111.88^P	71.12$^{(8)}$
Jaffeite	114.06	−6469.94^P	−6972.77^P	326.19	344.90^P	174.38$^{(8)}$

R: from the phase diagram refinement.
S: from solubility experiments.
P: estimated by using the polyhedral model.
Density from (1) Taylor [51]; (2) Merlino [109]; (3) Dent and Taylor [110]; (4) Merlino et al. [120]; (5) Wyckoff [111]; (6) Medaw [112]; (7) Dai and Post [113]; Anthony et al. [114]; Wolery [115].
Enthalpies of formation from (10) Newman [81]; (11) Zuern and Fehr [84].

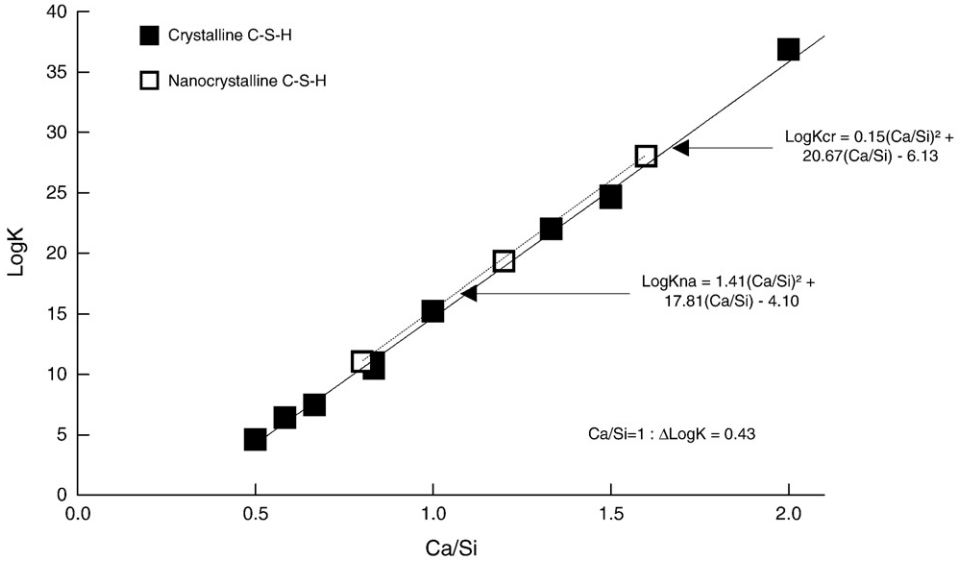

Fig. 9. Comparison of the 25 °C equilibrium constants of nanocrystalline and crystalline C–S–H.

this phase from 150 °C. In addition, Luke and Taylor [117], report the association xonotlite/truscottite from 200 °C while no gyrolite could be detected. Our calculations indicate a slightly low temperature for the first appearance of truscottite (135 °C instead of 150 °C), but this temperature remains reasonable and the phase relations are consistent with previous works.

The diagram in Fig. 12 indicates a large stability domain for jaffeite, decreasing the domains devoted to jennite, afwillite or hillebrandite. In that case, our model may overestimate the stability of jaffeite and among the possible explanations, we could emphasize the fact that the polyhedral decomposition model does not include a calibration phase with a Ca/Si > 2 whereas Ca/Si = 3 for jaffeite. However, Méducin et al. [118] have observed by ^{29}Si NMR the appearance of jaffeite at 120 °C, whereas neither hillebrandite nor C2SH,α have yet appeared. For Yanagisawa et al. [66], jaffeite could even appear between 200 and 300 °C but would be instable at such temperatures compared to calcio-chondrite. Anyway, this mineral has been observed in the natural state by Sarp and Peacor [78], in samples from the Kombat mine (Namibia). We can therefore conclude that jaffeite may verify the thermodynamic equilibrium and thus, could exhibit its own stability field. In addition, Sarp and Peacor [78] observe the coexistence with hillebrandite, which corresponds to the upper part of the diagram. On the other hand, it is still difficult to assess the results concerning the low temperature field, namely below 120 °C. The discussion remains open for this mineral and values reported in Table 9 must be considered as tentative values only.

The last phase to be tested is the hydrate C2SH,α. It is a rather common phase in experiments, for reaction temperature ranging between 120 and 160 °C [64,69] but, to our knowledge, it doesn't seems to have been found in a natural environment, yet. The calculation results, presented in Fig. 12, predict a reduced stability field, wedged between afwillite and jaffeite. This field is probably too strongly constrained by jaffeite. However, the transition with hillebrandite occurs in our case at 159 °C, which indeed corresponds to the observations of Assarsson and Rydberg [87] and Aitken and Taylor [69]. Finally, our calculations indicate the possible existence of this phase, replacing hillebrandite when the temperature drops below 159 °C.

Concerning foshagite, our results do not indicate a proper stability field at $T < 200$ °C, although Buick et al. [77] have observed this mineral coexisting with hillebrandite in samples from the Bushweld complex, South Africa. However, this phase seems to be less frequently observed in experiments than hillebrandite or xonotlite, for T < 200 °C [119]. For example, Ahmed and Taylor [68] observed the appearance of foshagite, coexisting with hillebrandite, at 180 °C after

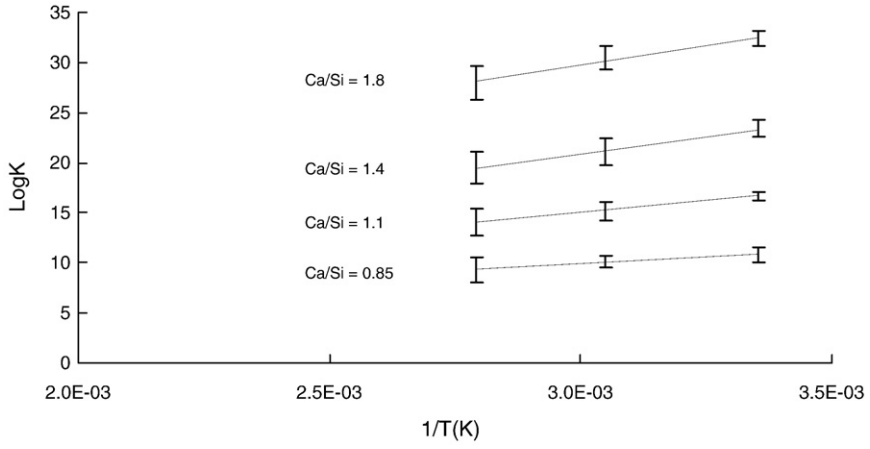

Fig. 10. Equilibrium constants of four nanocrystalline C–S–H, calculated using solution compositions from Glasser et al. [116].

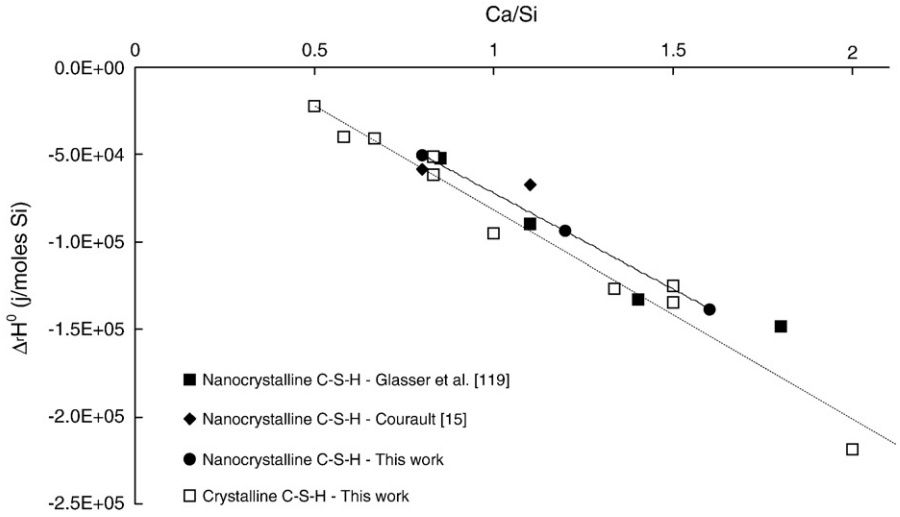

Fig. 11. Enthalpy of reaction of nanocrystalline and crystalline C–S–H, as a function of the Ca/Si ratio.

3 days of reaction. Then, after 14 days of reaction, this phase is progressively replaced by xonotlite whereas the association foshagite/hillebrandite subsists after 14 days at 250 °C. We can emphasize another hypothesis in order to explain the lack of an actual stability field for foshagite. The chemical formula we have adopted for foshagite is taken from Babushkin et al. [80] and it includes 0.5 mol of H_2O. However, although molecular water stabilizes low temperature phases, this is probably not the case for high temperature phases. Moreover, the formula presented by Black et al. [106] does not include molecular water.

5. Conclusions

The aim of the present study was to investigate the temperature dependency of the thermodynamic functions associated with the nanocrystalline and crystalline C–S–H phases. As regards to the nanocrystalline phases, we have calculated the composition and the equilibrium constant of three C–S–H phases (C/S = 1.6, 1.2 and 0.8), metastable with respect to crystalline C–S–H. In addition we have opened a discussion concerning the influence of elements other than Ca or Si in the considered chemical system. Such elements could have been incorporated into the solid phase, depending on the synthesis process. We have highlighted that these impurities could imply a displacement of the C–S–H solubility curve. This effect could also prevent a comparison between solubility models based on either a continuous or a fixed composition for nanocrystalline C–S–H.

The polyhedral decomposition model developed with the refined thermodynamic properties of crystalline C–S–H phases allows first to estimate the enthalpy of formation and the heat capacity of nanocrystalline C–S–H. Verifications indicate the consistency of predicted values with experimental results. In addition, the estimate for okenite and truscottite properties has enabled to complete the C–S–H phase diagram. For these phases, calculated phase relations globally agree with experimental and field observations. On the other hand, jaffeite seems to be strongly stabilized by model estimates, reducing the stability fields of afwillite and hillebrandite. Finally, in the case of the hydrate C2SH,α, the model could predict a transition with hillebrandite at 159 °C, in agreement with some already published results but against the hypothesis of its metastability. For those phases, a more accurate structural model, especially concerning the molecular water amount would allow the refinement of the relations between these phases.

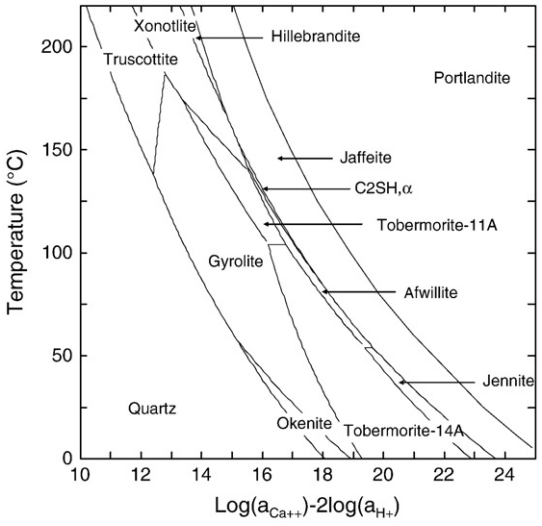

Fig. 12. Phase diagram in the $CaO–SiO_2–H_2O$ system, adding phases whose thermodynamic properties are estimated in this work.

Acknowledgements

This study was financially supported by ANDRA (Thermochimie Project) and BRGM (Project PDR07EPI54). The authors would like to thank Pr. D.M. Roy (The Pennsylvania State University) for her help in the literature review at the very beginning of the project. Two anonymous reviewers are acknowledged for their fruitful comments and suggestions that contributed strongly in improving the document.

References

[1] ANDRA, Evaluation de la faisabilité du stockage géologique en formation argileuse: ANDRA, Dossier 2005, Collection Les Rapports, 2005.
[2] P. Landais, Advances in geochemical research for the underground disposal of high-level, long-lived radioactive waste in a clay formation, J. Geochem. Explorat. 88 (2006) 32–36.
[3] F.P. Glasser, M. Atkins, Cements in radioactive waste disposal, Mater. Res. Soc. Bull. 19 (1994) 33–38.
[4] E.C. Gaucher, P. Blanc, Cement/clay interactions — a review: experiments, natural analogues, and modelling, Waste Manag. 26 (2006) 776–788.
[5] X. Bourbon, E. Giffaut, F. Plas, P. Bouniol, M. Carcasses, M. Landesman, B. Lothenbach, M. Ochs, J.P. Ollivier, I. Pointeau, P. Reiller, J. Smellie, C. Talerico, J.M. Torrenti, Référentiel matériaux. Tome 3: Les matériaux cimentaires, ANDRA Report C.RP.AMAT.01.060. ANDRA, Châtenay-Malabry France 2001.

[6] P. Blanc, P. Piantone, A. Lassin, A. Burnol, Thermochimie: Sélection de constantes thermodynamiques pour les éléments majeurs, le plomb et le cadmium., Rapport BRGM RP-54902-FR, 2006.
[7] P. Piantone, C. Nowak, P. Blanc, A. Lassin, A. Burnol, Themoddem: THERmodynamique et MOdélisation de la Dégradation DEchets Minéraux. Rapport BRGM BRGM/RP-54547-FR, 2006.
[8] F.P. Glasser, E.E. Lachowski, D.E. Macphee, Compositional model for calcium silicate hydrate (C–S–H) gels, their solubilities, and free energies of formation, J. Am. Ceram. Soc. 70 (1987) 481–485.
[9] F.P. Glasser, D.E. Macphee, E.E. Lachowski, Solubility modelling of cements: implications for radioactive waste immobilization, Mater. Res. Soc. Sympos. Porceed. 84 (1987) 331–341.
[10] H.M. Jennings, Aqueous solubility relationships for two types of calcium silicates hydrate, J. Amer. Ceram. Soc. 69 (1986) 614–618.
[11] U. Berner, A thermodynamic description of the evolution of pore water chemistry and uranium speciation during the degradation of cement, PSI-Bericht 62 Switzerland 1990.
[12] M. Kersten, Aqueous solubility diagrams for cementitious waste stabilization system. 1. The C–S–H solid solution system, Envir. Sci. Technol. 30 (1996) 2286–2293.
[13] C.L. Dickson, D.R.M. Brew, F.P. Glasser, Solubilities of $CaO–SiO_2–H_2O$ phases at 25° 55° and 85 °C, Adv. Cem. Res. 16 (2004) 35–43.
[14] F.P. Glasser, M. Paul, C.L. Dickson, D. Reed, Performance of cement barriers: experimental and modelling aspects, in barrier performance of cements and concretes in nuclear waste repositories, European Communities editors EURATOM Project report EUR 19780 EN 2001.
[15] A.C. Courault, Simulation experimentale des C–S–H dans les betons modernes: etude de la composition et des proprietes a l'equilibre dans des milieux complexes. PhD Thesis Université de Bourgogne (2000).
[16] M. Paul, F.P. Glasser, Impact of prolonged warm (85 degrees C) moist cure on Portland cement paste, Cem. Concr. Res. 30 (2000) 1869–1877.
[17] J.J. Thomas, J.J. Chen, D.A. Neumann, H.M. Jennings, Ca–OH bonding in the C–S–H gel phase of tricalcium silicate and white portland cement pastes measured by inelastic neutron spectroscopy, Chem. Mat. 15 (2003) 3813–3817.
[18] J.D. Cox, D.D. Wagman, V.A. Medvedev, CODATA key values for thermodynamics, New York Hemisphere Publishing Corporation 1989.
[19] V.A. Pokrovskii, H.C. Helgeson, Thermodynamic properties of aqueous species and the solubilities of minerals at high pressures and temperatures: the system $Al_2O_3–H_2O–NaCl$, Am. J. Sci. 295 (1995) 1255–1342.
[20] D.J. Rimstidt, Quartz solubility at low temperatures, Geochim. et Cosmochim. Acta 61 (1997) 2553–2558.
[21] H. Wanner, Guidelines for the review procedure and data selection, NEA TDB-1 Guidelines 2000 (www.nea.fr/html/dbtdb/guidelines).
[22] I. Grenthe, H. Wanner, Guidelines for the extrapolation to zero ionic strength, NEA TDB-2 Guidelines 2000 (www.nea.fr/html/dbtdb/guidelines).
[23] I. Puigdomenech, J.A. Rard, A.Y. Plyasunov, I. Grenthe, Temperature corrections to thermodynamic data and enthalpy calculations, NEA TBD-4 Guidelines 1999 (www.nea.fr/html/dbtdb/guidelines).
[24] H.C. Helgeson, D.H. Kirkham, G.C. Flowers, Theoretical prediction of the thermodynamic behavior of aqueous electrolytes at high pressures and temperatures: IV. Calculation of activity coefficients, osmotic coefficients, and apparent molal and standard and relative partial molal properties to 600°C and 5 kbar, Am. J. Sci. 281 (1981) 1249–1516.
[25] M.B. Ewing, T.H. Lilley, G.M. Olofsson, M.T. Ratzsch, G. Somsen, Standard quantities in chemical thermodynamics, Pure Appl. Chem. 66 (1994) 533–552.
[26] O.B. Fabrichnaya, S.K. Saxena, P. Richet, E.F. Westrum, Thermodynamic data, models and phase diagrams in multicomponent oxide systems, Springer, New York 2004.
[27] D.L. Parkhurst, C.A.J. Appelo, PHREEQC 2: a Computer Program for Speciation, Batch-reaction, One-dimensional Transport and Inverse Geochemical Calculations, USGS, Denver 2001.
[28] H.C. Helgeson, J.M. Delany, H.W. Nesbitt, D.K. Bird, Summary and critique of the thermodynamic properties of rock-forming minerals, Am. J. Sci. 278-A (1978).
[29] T.J. Wolery, C.F. Jove-Colon, Qualification of Thermodynamic Data for Geochemical Modeling of Mineral–Water Interactions in Dilute Systems, Report ANL-WIS-GS-000003 REV 00 2004.
[30] W. Hummel, U. Berner, E. Curti, F.J. Pearson, T. Thoenen, Nagra/PSI Chemical Thermodynamic Data Base 01/01, Universal Publishers, Parkland Florida USA 2002.
[31] I. Gunnarsson, S. Arnorsson, Nanocrystalline silica solubility and the thermodynamic properties of H4SiO4 in the range of 0° to 350 °C at Psat, Geochim. et Cosmochim. Acta 64 (2000) 2295–2307.
[32] A. Stephansson, Dissolution of primary minerals of basalt in natural waters I. Calculation of mineral solubilities from 0 °C to 350 °C, Chem. Geol. (2001) 225–250.
[33] M.D. Schulte, E.L. Shock, R.H. Wood, The temperature dependence of the standard-state thermodynamic properties of aqueous nonelectrolytes, Geochim. et Cosmochim. Acta 65 (2001) 3919–3930.
[34] E.L. Shock, H.C. Helgeson, Calculation of the thermodynamic and transport properties of aqueous species at high pressures and temperatures: Correlation algorithms for ionic aqueous species and equation of state predictions to 5 kb and 1000 °C, Geochim. et Cosmochim. Acta 52 (1988) 2009–2036.
[35] E.L. Shock, D.C. Sassani, M. Willis, D.A. Sverjensky, Inorganic species in geologic fluids: correlations among standard molal thermodynamic properties of aqueous ions and hydroxide complexes, Geochim. et Cosmochim. Acta 61 (1997) 907–950.
[36] S.L. Phillips, F.V. Hale, L.F. Silvester, M.D. Siegel, Thermodynamic Tables for Nuclear Waste Isolation, an Aqueous Solutions Database, Report NUREG/CR-4864 LBL-22860 SAND87-0323, Lawrence Berkeley Laboratory, Berkeley California 1988.
[37] D. Sverjensky, E.L. Shock, H.C. Helgeson, Prediction of the thermodynamic properties of aqueous metal complexes to 1000 °C and 5 kbar, Geochim. et Cosmochim. Acta 61 (1997) 1359–1412.
[38] D.D. Wagman, W.H. Evans, V.B. Parker, R.H. Schumm, I. Halow, S.M. Bailey, K.L. Churney, R.L. Nuttall, The NBS tables of chemical thermodynamic properties: selected values for inorganic and C1 and C2 organic substances in SI units, J. Phys. Chem. Reference Data 11 (2) (1982).
[39] I. Grenthe, J. Fuger, R.J.M. Konings, R.J. Lemire, A.B. Muller, C. Nguyen-Trung, H. Wanner, Chemical Thermodynamics of Uranium, North-Holland, Amsterdam 1992.
[40] W. Wagner, A. Pruss, The IAPWS Formulation 1995 for the thermodynamic properties of ordinary water substance for general and scientific use, J. Phys. Chem. Reference Data 31 (2002) 387–535.
[41] M. Atkins, F.P. Glasser, I.P. Moron, J.J. Jack, Thermodynamic modelling of blended cements at elevated temperature (50–90 °C), DOE-HMIP-94-001 Washington District of Columbia D.O.E 1994.
[42] J.J. Thomas, D. Rothstein, H.M. Jennings, B.J. Christensen, Effect of hydration temperature on the solubility behavior of Ca-, S-, Al-, and Si-bearing solid phases in Portland cement pastes, Cem. Concr. Res. 33 (2003) 2037–2047.
[43] J.J. Chen, J.J. Thomas, H.F.W. Taylor, H.M. Jennings, Solubility and structure of calcium silicate hydrate, Cem. Concr. Res. 34 (2004) 1499–1519.
[44] C.J. Bruton, A. Meike, B.E. Viani, S. Martin, B.L. Phillips, Thermodynamic and structural characteristics of cement minerals at elevated temperature, Report UCRL-JC-114116, 1994.
[45] S.U. Al-Dulaijan, G. Parry-Jones, A.H.J. Al-Tayyib, A.I. Al-Mana, ^{29}Si magic-angle-spinning nuclear magnetic resonance study of hydrated cement paste and mortar, J. Amer. Ceram. Soc. 73 (1990) 736–739.
[46] E.P. Flint, L.S. Wells, Study of the system $CaO–SiO_2–H_2O$ and of the reaction of water on the anhydrous calcium silicates, J. Res. Nat. Bureau of Standards, A, Phys. Chem. 12 (1934) 751–783.
[47] S.A. Greenberg, T.N. Chang, Investigations of the colloidal hydrated calcium silicates II. Solubility relationships in the calcium oxide–silica–water system at 25 °C, The Journal of Physical Chemistry 69 (1965) 182–188.
[48] M. Grutzeck, A. Benesi, B. Fanning, Silicon-29 magic angle spinning nuclear magnetic resonance study of calcium silicate hydrates, J. Amer. Ceram. Soc. 72 (1989) 665–668.
[49] D. Damidot, F.P. Glasser, Investigation of the $CaO–Al_2O_3–SiO_2–H_2O$ system at 25 °C by thermodynamic calculations, Cem. Concr. Res. 25 (1995) 22–28.
[50] H.F.W. Taylor, Hydrated calcium silicates, part I: compound formation at ordinary temperatures, J. Chem. Soc. 726 (1950) 3682–3690.
[51] H.F.W. Taylor, Cement Chemistry, 1st ed.Academic Press, London 1990.
[52] S.A. Stronach, F.P. Glasser, Modelling the impact of abundant geochemical components on phase stability and solubility of the $CaO–SiO_2–H_2O$ system at 25 °C: Na^+, K^+, SO_4^{2-}, Cl^- and CO_3^{2-}, Adv. Cem. Res. 36 (1997) 167–181.
[53] P.S. Roller, G. Ervine, The system calcium oxide–silica–water at 30 °C. The association of silicate ion in dilute alkaline solution, J. Chem. Soc. 62 (1940) 461–471.
[54] K. Fuji, W. Kondo, Heterogeneous equilibrium of calcium silicate hydrate in water at 30 °C, J. Chem. Soc., Dalton Transact. 2 (1981) 645–651.
[55] G.L. Kalousek, Application of different thermal analysis in a study of the system lime–silica–water, Proceeding of the 3rd International Symposium on Chemistry of Cements London, 1952.
[56] M. Atkins, F.P. Glasser, A. Kindness, Cement hydrate phases: solubility at 25 °C, Cem. Concr. Res. 22 (1992) 241–246.
[57] E.J. Reardon, An ion interaction model for the determination of chemical equilibria in cement/water systems, Cem. Concr. Res. 20 (1990) 175–192.
[58] D.K. Nordstrom, L.N. Plummer, D. Langmuir, E. Busenberg, H.M. May, B.F. Jones, D.L. Parkhurst, Revised chemical equilibrium data for major water–mineral reactions and their limitations, in: R.L. Bassett, D. Melchior (Eds.), Chemical modeling in aqueous systems II, American Chemical Society Symposium Series, vol. 416, 1990, pp. 398–413.
[59] P. Blanc, A. Bieber, B. Fritz, J. Duplay, A short range interaction model applied to illite/smectite mixed-layer minerals, Phys. Chem. Miner. 24 (1997) 574–581.
[60] P.D. Glynn, E.J. Reardon, Solid-solution aqueous solution equilibria: thermodynamic theory and representation, Am. J. Sci. 290 (1990) 164–201.
[61] C.I. Steefel, P.C. Lichtner, Multicomponent reactive transport in discrete fractures II: infiltration of hyperalkaline groundwater at Maqarin. Jordan, a natural analogue site, J. Hydrol. 209 (1998) 200–224.
[62] I. Harker, Dehydration series in the system $CaSiO_3–SiO_2–H_2O$, J. Amer. Ceram. Soc. 47 (1964) 521–529.
[63] D.M. Roy, Studies in the system $CaO–Al_2O3–SiO_2–H_2O$ IV: phase equilibria in the high lime portion of the system $CaO–SiO_2–H_2O$, Am. Mineral. 43 (1958) 1009–1028.
[64] G.O. Assarasson, Hydrothermal reactions between calcium hydroxide and nanocrystalline silica; the reactions between 180 and 220 °C, J. Phys. Chem. 61 (1957) 473–479.
[65] R. Jauberthie, M. Temimi, M. Laquerbe, Hydrothermal transformation of tobermorite gel to 10 Å tobermorite, Cem. Concr. Res. 26 (1996) 1335–1339.
[66] K. Yanagisawa, X. Hu, A. Onda, K. Kajiyoshi, Hydration of β-dicalcium silicate at high temperatures under hydrothermal conditions, Cem. Concr. Res. 36 (2006) 810–816.
[67] X.L. Hu, K. Yanagisawa, A. Onda, K. Kajiyoshi, Stability and phase relations of dicalcium silicate hydrates under hydrothermal conditions, J. Ceram. Soc. Jap. 114 (2006) 174–179.

[68] A.H.M. Ahmed, H.F.W. Taylor, The lime–silica–water system: equilibria at bulk calcium/silicon ratios of 1.5–2.5 at 180–250 °C, J. Appl. Chem. 19 (1969) 245–246.
[69] A. Aitken, H.F.W. Taylor, Hydrothermal reactions in lime–quartz pastes, J. Appl. Chem. 10 (1960) 7–15.
[70] J.A. Gard, K. Luke, H.F.W. Taylor, The crystal structure of K-phase $Ca_7Si_{16}O_{40}H_2$, Kristallografiya 26 (1981) 1218–1223.
[71] J.A.T. Smellie, Maqarin Natural Analogue Project, Phase IV: Reconnaissance Mission Report (April 28th to May 7th 1999), SKB Report R-00-34 2000.
[72] I. Kusachi, C. Henmi, K. Henmi, Afwillite and jennite from Fuka, Okayama Prefecture, Japan, Mineral. J. 14 (1989) 279–292.
[73] R.N. Sukheswala, R.K. Avasia, M. Gangopadhyay, Zeolites and associated minerals in the Deccan Traps of western India, Mineral. Mag. 39 (1974) 658–671.
[74] T.E.C. Keith, L.W. Staples, Zeolites in Eocene basaltic pillow lavas of the Siletz river volcanic Central Coast range, Oregon, Clays Clay Miner. 33 (1985) 135–144.
[75] J.P. Rançon, Hydrothermal history of Piton des Neiges volcano (Reunion Island, Indian Ocean), J. Volcanol. Geotherm. Res. 26 (1985) 297–305.
[76] K.L. Rogers, P.S. Neuhoff, A.K. Pedersen, D.K. Bird, CO2 metasomatism in a basalt-hosted petroleum reservoir, Nuussuaq, West Greenland, Lithos 92 (2006) 55–82.
[77] S.I. Buick, R. Gibson, T. Wallmach, J. Metz, The occurrence of cuspidine, foshagite and hillebrandite in calc-silicate xenoliths from the Bushveld complex, South Africa, South Afric. J. Geol. 103 (2000) 249–254.
[78] H. Sarp, D.R. Peacor, Jaffeite, a new hydrated calcium silicate from the Kombat mine, Namibia, Am. Mineral. 74 (1989) 1203–1206.
[79] K.E. Bargar, R.C. Erd, T.E.C. Keith, M.H. Beeson, Dachiardite from Yellowstone National Park, Wyoming, Can. Mineral. 25 (1987) 475–483.
[80] V.I. Babushkin, G.M. Matveyev, O.P. Mchedlov-Petrossyan, Thermodynamics of Silicates, Springer-Verlag, Berlin 1985.
[81] E. Newman, Heats of formation of xonotlite, hillebrandite, and foshagite, J. Res. Nat. Bureau Stand. 57 (1956) 27–30.
[82] M.W.J. Chase, NIST-JANAF Thermochemical Tables, J. Phys. Chem. Refer. Data 9 (1998).
[83] D. Savage, C. Walker, R. Arthur, C. Rochelle, C. Oda, H. Takase, Alteration of bentonite by hyperalkaline fluids: a review of the role of secondary minerals, Physics and Chemistry of the Earth, Parts A/B/C 32 (2007) 287–297.
[84] S.G. Zuern, K.T. Fehr, Phase relations and thermodynamic properties of 1.13 nm tobermorite and xonotlite, Sixth International Symposium on Hydrothermal reactions/Fourth International Conference on Solvo-thermal Reactions Kochi Japan (2000) 286–289.
[85] J.E. Taylor, The heat of formation of xonotlite, tobermorite, hillebrandite and afwillite, Conference on the Silicate Industry, Akad Kiado Budapest Hungary, 1968, pp. 179–184.
[86] T. Maeshima, H. Noma, M. Sakiyama, T. Mitsuda, Natural 1.1 and 1.4 nm tobermorites from Fuka, Okayama, Japan: chemical analysis, cell dimensions, ^{29}Si NMR and thermal behavior, Cem. Concr. Res. 33 (2003) 1515–1523.
[87] G.O. Assarasson, E.R. Rydberg, Hydrothermal reactions between calcium hydroxide and nanocrystalline silica, J. Phys. Chem. 60 (1956) 397–404.
[88] K. Speakman, The stability of tobermorite in the system $CaO–SiO_2–H_2O$ at elevated temperature and pressures, Mineral. Mag. 36 (1968) 1090–1103.
[89] S.Y. Hong, F.P. Glasser, Phase relations in the $CaO–SiO_2–H_2O$ system to 200 °C at saturated steam pressure, Cem. Concr. Res. 34 (2004) 1529–1534.
[90] S.A.S. El-Hemaly, T. Mitsuda, H.F.W. Taylor, Synthesis of normal and anomalous tobermorites, Cem. Concr. Res. 7 (1977) 429–438.
[91] R.G. Berman, Internally-consistent thermodynamic data for stoichiometric minerals in the system $Na_2O–K_2O–CaO–MgO–FeO–Al_2O_3–SiO_2–TiO_2–H_2O–CO_2$, J. Petrol. 29 (1988) 445–522.
[92] T.J.B. Holland, R. Powell, An internally-consistent thermodynamic data set for phases of petrological interest, J. Metamor. Geol. 16 (1998) 309–343.
[93] L. Heller, H.F.W. Taylor, Hydrated calcium silicates: part IV, J. Chem. Soc. 480 (1952) 2535–2541.
[94] A. Atkinson, A.W. Harris, J.A. Hearne, Hydrothermal alteration and ageing of synthetic calcium silicate hydrate gels, NIREX NSS/R/374 1995.
[95] G.L. Kalousek, E.B. Nelson, Hydrothermal reactions of dicalcium silicate and silica, Cem. Concr. Res. 8 (1978) 283–289.
[96] E. Revertegat, F. Adenot, C. Richet, L. Wu, F.P. Glasser, D. Damidot, S.A. Stronach, Theoretical and experimental study of degradation mechanisms of cement in the repository environment, EUR 17642 EN 1997.
[97] D.M. Roy, E.L. White, C.A. Langton, M.W. Grutzeck, New High Temperature Cementing Materials for Geothermal Wells: Stability and Properties, Report BNL-51249 1980.
[98] A.K. Sarkar, M.W. Barnes, D.M. Roy, Longevity of borehole and shaft sealing materials: thermodynamic properties of cements and related phases applied to repository sealing office of nuclear waste: Isolation Technical Report, ONWI 201 1981.
[99] N. Akinfiev, A. Zotov, Thermodynamic description of equilibria in mixed fluids (H_2O-non-polar gas) over a wide range of temperature (25–700 °C) and pressure (1–5000 bars), Geochim. et Cosmochim. Acta 63 (1999) 2025–2041.
[100] G.R. Robinson, J.L. Haas, Heat capacity, relative enthalpy, and calorimetric entropy of silicate minerals: an empirical method of prediction, Am. Mineral. 68 (1983) 541–553.
[101] J.A. Chermak, J.D. Rimstidt, Estimating the thermodynamic properties (ΔGf^0) of silicate minerals at 298 K from the sum of polyhedral contributions, Am. Mineral. 74 (1989) 1023–1031.
[102] A. La Iglesia, J.F. Félix, Estimation of thermodynamic properties of mineral carbonates at high and low temperatures from the sum of polyhedral contributions, Geochim. et Cosmochim. Acta 58 (1994) 3983–3991.
[103] Y. Tardy, R.M. Garrels, Prediction of Gibbs free energies of formation—I. Relationships among Gibbs free energies of formation of hydroxides, oxides and aqueous ions, Geochim. et Cosmochim. Acta 40 (1976) 1051–1056.
[104] Y. Tardy, R.M. Garrels, Prediction of Gibbs free energies of formation—II. Monovalent and divalent metal silicates, Geochim. et Cosmochim. Acta 41 (1977) 87–92.
[105] L. Black, K. Garbev, P. Stemmermann, K.R. Hallam, G.C. Allen, X-ray photoelectron study of oxygen bonding in crystalline C–S–H phases, Phys. Chem. Miner. 31 (2004) 337–346.
[106] L. Black, A. Stumm, K. Garbev, P. Stemmermann, K.R. Hallam, G.C. Allen, X-ray photoelectron spectroscopy of the cement clinker phases tricalcium silicate and β-dicalcium silicate, Cem. Concr. Res. 33 (2003) 1561–1565.
[107] X. Cong, R.J. Kirkpatrick, ~(29)Si MAS NMR study of the structure of calcium silicate hydrate, Adv. Cem. Based Mater. 3 (1996) 144–156.
[108] L. Mercury, P. Vieillard, Y. Tardy, Thermodynamic of ice polymorphs and "ice-like" water in hydrates and hydroxides, Appl. Geochem. 16 (2001) 161–181.
[109] S. Merlino, Gyrolite: its crystal structure and crystal chemistry, Mineral. Mag. 52 (1988) 377–387.
[110] L.S. Dent, H.F.W. Taylor, The dehydration of xonotlite, Acta Crystallographica 9 (1956) 1002–1004.
[111] R.W.G. Wyckoff, Crystal Structures, Second Edition Tome 4, Interscience Publishers, New York 1963.
[112] H.D. Megaw, C.H. Kelsey, Crystal structure of tobermorite, Nature 177 (1956) 390–391.
[113] Y. Dai, J.E. Post, Crystal structure of hillebrandite: a natural analogue of calcium silicate hydrate (C–S–H) phases in Portland cement, Am. Mineral. 80 (1995) 841–844.
[114] J.W. Anthony, R.A. Bideaux, K.W. Bladh, M.C. Nichols, Handbook of Mineralogy, Volume II. Silica, Silicates, Mineral Data Publishing, Tucson 1995.
[115] T.J. Wolery, EQ3NR, a Computer Program for Geochemical Aqueous Speciation-solubility Calculations: Theoretical Manual, Users Guide and Related Documentation (version 7.0). Lawrence Livermore Laboratory URCL-53414 1992.
[116] F.P. Glasser, M. Tyrer, K. Quillin, D. Ross, J. Pedersen, K. Goldthorpe, D. Bennett, M. Atkins, The chemistry of blended cements and backfills intended for use in radioactive waste disposal, Research and Development Technical Report P98, UK Environment Agency 1998.
[117] K. Luke, H.F.W. Taylor, Equilibria and non-equilibria in the formation of xonotlite and truscottiten, Cem. Concr. Res. 14 (1984) 657–662.
[118] F. Méducin, B. Bresson, N. Lequeux, M. de Noirfontaine, H. Zanni, Calcium silicate hydrates investigated by solid-state high resolution ^1H and ^{29}Si nuclear magnetic resonance, Cem. Concr. Res. 37 (2007) 631–638.
[119] I. Kaprálik, L. Stevula, J. Petrovic, F. Hanic, Study of the system $CaO–SiO_2–CO_2–H_2O$ in relation to scawtite under hydrothermal conditions, Cem. Concr. Res. 14 (1984) 866–872.
[120] S. Merlino, E. Bonaccorsi, T. Armbruster, The real structures of clinotobermorite and tobermorite 9: OD character, polytypes, and structural relationships, Eur. J. Mineral. 12 (2000) 411–429.
[121] B. Lothenbach, T. Matschei, G. Möschner, F.P. Glasser, Thermodynamic modelling of the effect of temperature on the hydration and porosity of Portland cement, Cem. Concr. Res. 38 (2008) 1–18.
[122] W.F. Cole, C.J. Lancucki, Products formed in an aged concrete the occurrence of okenite, Cem. Concr. Res. 13 (1983) 611–618.
[123] T. Matschei, B. Lothenbach, F.P. Glasser, Thermodynamic properties of Portland cement hydrates in the system $CaO–Al_2O_3–SiO_2–CaSO_4–CaCO_3–H_2O$, Cem. Concr. Res. 37 (2007) 1379–1410.
[124] B. Lothenbach, T. Matschei, G. Möschner, F.P. Glasser, Thermodynamic modelling of the effect of temperature on the hydration and porosity of Portland cement, Cem. Concr. Res. 38 (2008) 1–18.
[125] C.S. Walker, D. Savage, M. Tyrer, K.V. Ragnarsdottir, Non-ideal solid solution aqueous solution modeling of synthetic calcium silicate hydrate, Cem. Concr. Res. 37 (2007) 502–511.